Title
A METHOD FOR DETERMINING THE SOLUBILITY OF HYDROGEN IN MOLTEN ALUMINUM-LITHIUM ALLOYS

Author
Verma, T.

Publication Date
1988-08-01

Center for Advanced Materials

CAM

A Method for Determining the Solubility of Hydrogen in Molten Aluminum-Lithium Alloys

T. Verma
(M.S. Thesis)

August 1988

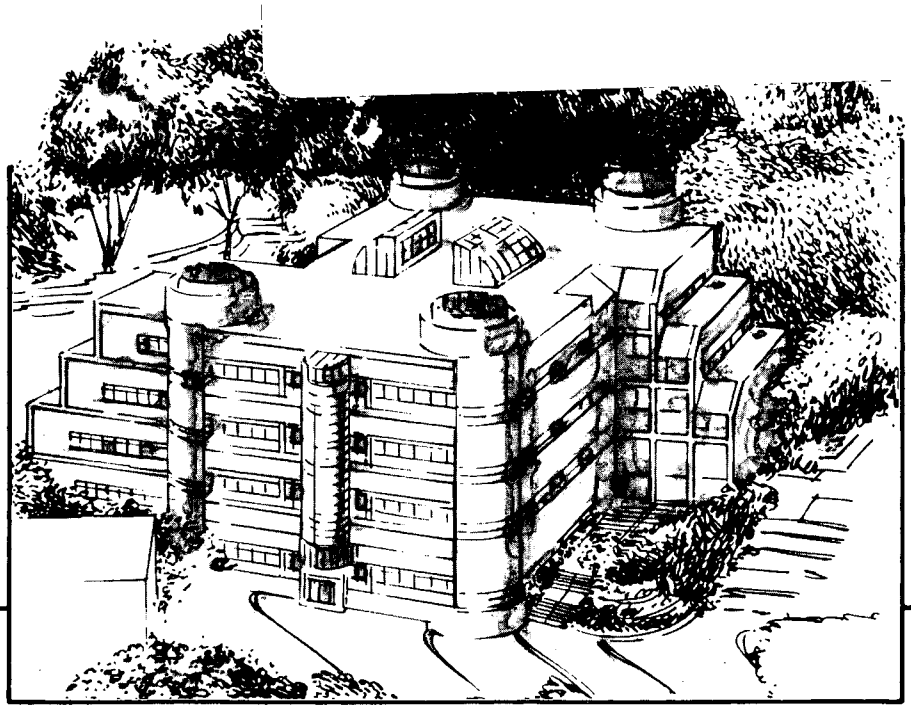

Materials and Chemical Sciences Division

Lawrence Berkeley Laboratory • University of California

ONE CYCLOTRON ROAD, BERKELEY, CA 94720 • (415) 486-4755

Prepared for the U.S. Department of Energy under Contract DE-AC03-76SF00098

DISCLAIMER

LBL-24512

A METHOD FOR DETERMINING THE SOLUBILITY OF HYDROGEN IN MOLTEN ALUMINUM-LITHIUM ALLOYS

Tarun Verma
Lawrence Berkeley Laboratory
University of California
Berkeley, CA 94720

This work was supported by the Director, Office of Energy Resources, Office of Basic Energy Sciences, Materials Sciences Division of the U.S. Department of Energy under Contract No. DE-AC03-76SF00098.

A Method for Determining the Solubility of Hydrogen in Molten Aluminum-Lithium Alloys

Tarun Verma

ABSTRACT

A constant volume technique, involving the measurement of differential pressure generated between a control volume subjected to an inert gas and an "active" volume subjected to hydrogen, has been used to determine the solubility of hydrogen in molten 2090 aluminum lithium alloys. The solubility of hydrogen in 2090 aluminum lithium alloys obeys Sievert's law and lies between 1-6 ppm for pressures varying from 250-950 mm Hg in the temperature range 650-750^{o}C. The heat of dissolution of hydrogen is of the order of 135 kJ mol^{-1} in this alloy.

TABLE OF CONTENTS

LIST OF FIGURES

ACKNOWLEDGMENTS

I would like to take this opportunity to express my heartfelt gratitude and thanks to my advisor, Professor J. W. Evans for his continued encouragement and guidance throughout the duration of this investigation, especially for his patience and understanding during the initial stages of the design and fabrication of the experimental setup.

Thanks are also due to Charlie, Felix and Ken at the machine shop, John and Ron at the electronics shop and Tom at the glassblowing shop without whom this investigation would not have seen the light of day.

I would also like to acknowledge with sincere thanks, the assistance and help of Eve, the secretary of our research group, in the preparation of this manuscript and for her moral support throughout.

Finally, I would like to thank the faculty, staff and fellow students who have made my stay at Berkeley a most rewarding and pleasant experience.

1. INTRODUCTION

The dissolution of gases in metals and alloys is a well documented phenomenon (1) which has been shown to affect the mechanical properties of materials, in most cases adversely. In particular, hydrogen appears to be the principal gas in light metals (2). During metal casting, hydrogen may be generated both by thermal dissociation of water and by reaction of water with the metal in question; hydrogen then diffuses into the metal. The solubility of hydrogen in aluminum and its alloys, materials widely used in the aerospace and ground transportation industries, has been studied (3-13). In the past few years, aluminum lithium alloys have assumed increasing importance in the industry owing to their superior mechanical properties. However, published data on the solubility of hydrogen in these alloys is not widely available.

Therefore, the objective of this experimental investigation is to design and validate a method to determine the solubility of gases in molten alloy systems, and specifically, to generate data on the solubility of hydrogen in liquid aluminum lithium alloys.

2. A BRIEF OVERVIEW OF ALUMINUM-LITHIUM ALLOYS

2.1 General introduction

In 1983, two of the largest producers of aluminum alloys for the aerospace industry - the British Alcan Aluminum concern and the American giant ALCOA - announced the introduction of a new and revolutionary material - the aluminum lithium alloy. This material is considered to be the most important development in aluminum alloys since the introduction of Al-7075 (high strength aluminum zinc alloy), as it offers competition to advanced carbon-of-aramid fibre reinforced plastics (14). They claim that the usage of this material in existing aircraft designs would result in mass savings of 10% and if used for new aircraft designs, mass savings of 15-20% are possible.

Lithium is one of the eight elements which have more than 1 atomic % solubility in aluminum. Only three other elements (copper, magnesium and zinc) have as high a solubility in aluminum. Lithium is the lightest metallic element and the only one (except beryllium) which, when alloyed with aluminum, increases the elastic modulus and decreases the density (magnesium decreases the elastic modulus). For every mass % lithium added to aluminum, the density is reduced by 3% and the elastic modulus (up to a lithium content of 4%) is increased by 6%. The specific elastic modulus,

E/ρ, is increased by decreasing density while increasing elastic modulus (15).

From the economic point of view, the mass savings achieved by using aluminum lithium alloys can be realized in the following ways:

1. The lower aircraft mass means lower fuel consumption; this translates into fuel savings of $650-900 per kilogram mass reduction per annum;
2. The lower aircraft mass can also be used to increase the maximum payload, or the maximum range of the aircraft, which will yield higher revenues (14).

2.2 Metallurgical Fundamentals

The phase diagram of the aluminum lithium alloy system is shown in Fig. 2.1 (16). An extensive overview of the precipitation behavior of the aluminum lithium alloy system has been published (17). Binary aluminum lithium alloys with more than 5 atomic % (1.35 mass %) lithium, when quenched from the single phase field and aged at room temperature or higher, decompose into a two phase alloy containing the metastable Al_3Li (δ') phase and the matrix. These precipitates are coherent with the aluminum lattice, spherical and in contrast to other metastable phases in Al-Cu and Al-Zn alloys, are ordered. The crystal structure corresponds to the Ll_2 (ordered Cu_3Au structure) type and there is only a small mismatch between the aluminum lattice and

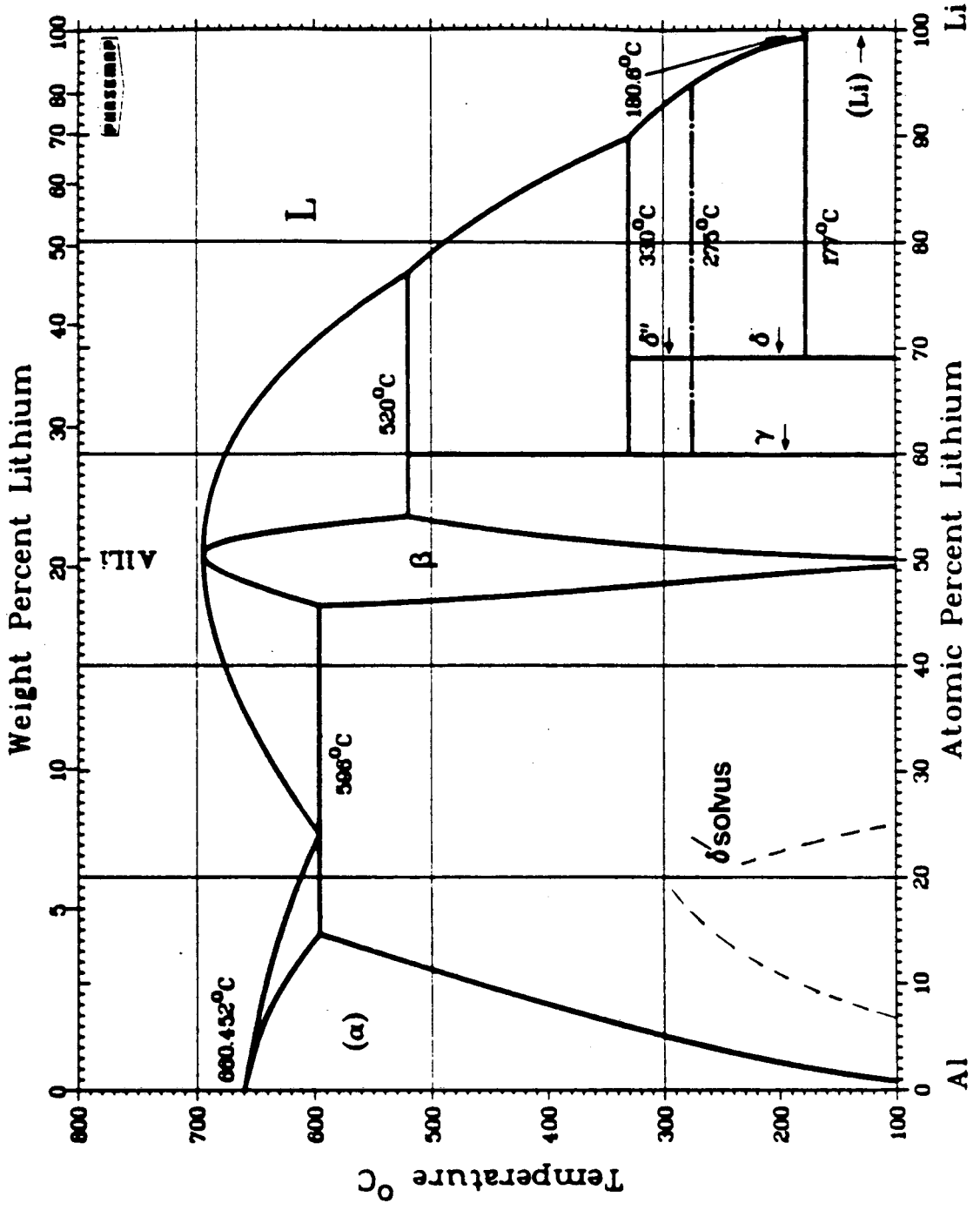

Fig. 2.1 Aluminum-lithium phase diagram

NOTE: The exact location of the δ' solvus line is not yet completely clear (14).

the δ' lattice.

For ternary alloys containing copper (the alloy used in this investigation is 2090 Al-Li which is a 2.2 mass% Cu-2.1 mass% Li), there are several precipitation sequences which are partly related to the binary Al-Cu system and partly to the Al-Li system:

Supersaturated Solid Solution (SSS) $\longrightarrow$ GP Zones $\longrightarrow$ θ'' Phase $\longrightarrow$ θ' $\longrightarrow$ θ

Supersaturated Solid Solution (SSS) $\longrightarrow$ T_1

Supersaturated Solid Solution (SSS) $\longrightarrow$ δ' $\longrightarrow$ δ

The stable T_1 (Al_2CuLi) phase is hexagonal (a = 4.97°A, c = 9.34°A), with its basal plane parallel to the {111} plane of the aluminum lattice. This phase is partly coherent. The formation of the various phases depends on the Cu:Li ratio - for 2090 alloys the T_1 phase alloy occurs at all aging temperatures along with the δ' phase.

2.3 Production techniques

Aluminum lithium alloys are most commonly produced through the ingot metallurgy process (IM-process). The semi-continuous direct-chill method is used. In this method, the bottom of the mould moves downwards as soon as the mould surface is solidified and strong enough to support the pool of liquid material above it. Watercooling is used to cool down the molten alloy. This is where most of the hydrogen is formed and dissolved. The cast ingots can be rolled into

plates or sheets. The number of successive heat treatments is limited, because of the possibility that lithium diffuses to the plate surface and is oxidized there (18). Compared to other methods, the IM process is relatively inexpensive and large size ingots are possible. However, casting facilities are costly and special precautions must be taken against explosion.

Aluminum lithium alloys may also be produced through the powder metallurgy (PM) process, in which molten material is atomized by a high velocity air stream (or an inert gas such as argon or helium). Cooling rates of 10^3 to 10^6 $^{o}C/sec$ are possible with this method. The resulting powder is put into a container, degassed and hot compacted. The container is then removed by milling and the billet can be used for forgings and extrusions or rolled into sheets and plates. An important advantage of the PM process is that it gives a greater flexibility in composition and microstructure. Supersaturation with alloying elements is possible without segregation effects that may occur in the IM process. With the PM process it is also possible to use alloying elements that normally cannot be used because of their low solubility in the solid state.

A third process for producing aluminum lithium alloys is splat-cooling, a variant of the PM process. In splat-cooling, a small stream of molten metal falls on a rapidly

rotating wheel. The molten metal solidifies on the wheel and results in a very thin ribbon with a thickness of some 20 to 50 μm and a width of some mm. The ribbons can be compacted and degassed to form ingots. This is safer than the PM technique but only small ingot sizes are possible.

For commercial purposes, the IM process is the one in vogue, primarily because there already exists a production line for the preparation of aluminum alloys and only small modifications are needed for their manufacture. The other techniques are still in the experimental stages.

2.4 Specific Issues Relating to Aluminum Lithium Alloys

Owing to the emergence of the aluminum lithium alloy system as a potential replacement for conventional aluminum alloys in the aerospace and ground transportation industry, extensive research has been done on this alloy system. Three international conferences on these alloys have been held since 1980 and the proceedings are available (19-21). However, most of the research has been oriented towards the physical metallurgical aspects of these alloys; there are relatively few papers dealing with their processing, and most of this work has been done by the industry and is proprietary knowledge. The following paragraphs attempt to summarize the findings of earlier investigators.

The casting of aluminum lithium alloys is known to pose many problems (22). Lithium reactivity with oxygen and

moisture makes it difficult to cast the alloys in air (23). Porosity develops even when the melt has been covered with flux or an inert gas blanket. Impurity levels (of oxygen, water vapor and carbon dioxide) of 100 ppm in the gases used are sufficient to cause oxidation and oxide entrapment.

Researchers at Imperial College, London, have done considerable work on the reactivity of oxygen with aluminum lithium alloys (24-26). They have found that oxidation of aluminum alloys containing lithium results in the formation of thick, friable, non-protective oxide films after relatively short oxidation times. The films are composed of the tetragonal spinel γ-$LiAlO_2$ which develops as the primary phase at the metal/oxide interface. With alloys containing both lithium and magnesium, magnesium oxidation may predominate at early stages, particularly in wet environments. Oxidation in moist atmospheres also leads to severe oxide eruptions, intergranular oxidation after the development of raised surface grains and complete intergranular disintegration and loss of alloy integrity.

Oxidation is not limited by lithium diffusion but controlled by the nucleation and growth of crystalline reaction products at the metal/oxide interface. Irrespective of the reacting gas, the reaction rate is controlled by the water vapor level.

In the case of liquid alloys, the amounts of oxygen,

water vapor and carbon dioxide impurities of the furnace atmospheres control surface reactions with the formation of Li_2O, $LiOH \cdot H_2O$ and Li_2CO_3 phases. Oxidation weight gain in Al-Li melts is rapid even when the oxygen and water vapor levels are as low as 30 ppm. Only by the use of high purity furnace gases can lithium loss due to chemical reactions be minimized. Fig. 2.2 shows the Ellingham diagram relevant to Al-Li alloys and it is obvious that all kind of surface reactions are thermodynamically feasible.

It is thought that the presence of hydrogen in aluminum lithium alloys may be connected with poor alloy ductility and fracture toughness (27). One hypothesis for this connection is that the poor ductility of these alloys may be due to the formation of a stable hydride of aluminum or aluminum and lithium, such as LiH or Li_3AlH_6. This has been surmised from the fact that aluminum lithium alloys are reported to contain more than 10 times the amount of hydrogen normally observed in high-strength aluminum-based alloys and that lithium hydride is the most stable of all alkali-metal hydrides. Hydrogen contamination occurs during the processing of these alloys and is most severe near the surface, though significant penetration into the alloy has also been observed. This entrapped hydrogen is not amenable to vacuum annealing as this causes lithium loss.

From the above discussion, it is clear that there is

still insufficient knowledge regarding the processing of aluminum lithium alloys and that there is abundant scope for scientific enquiry.

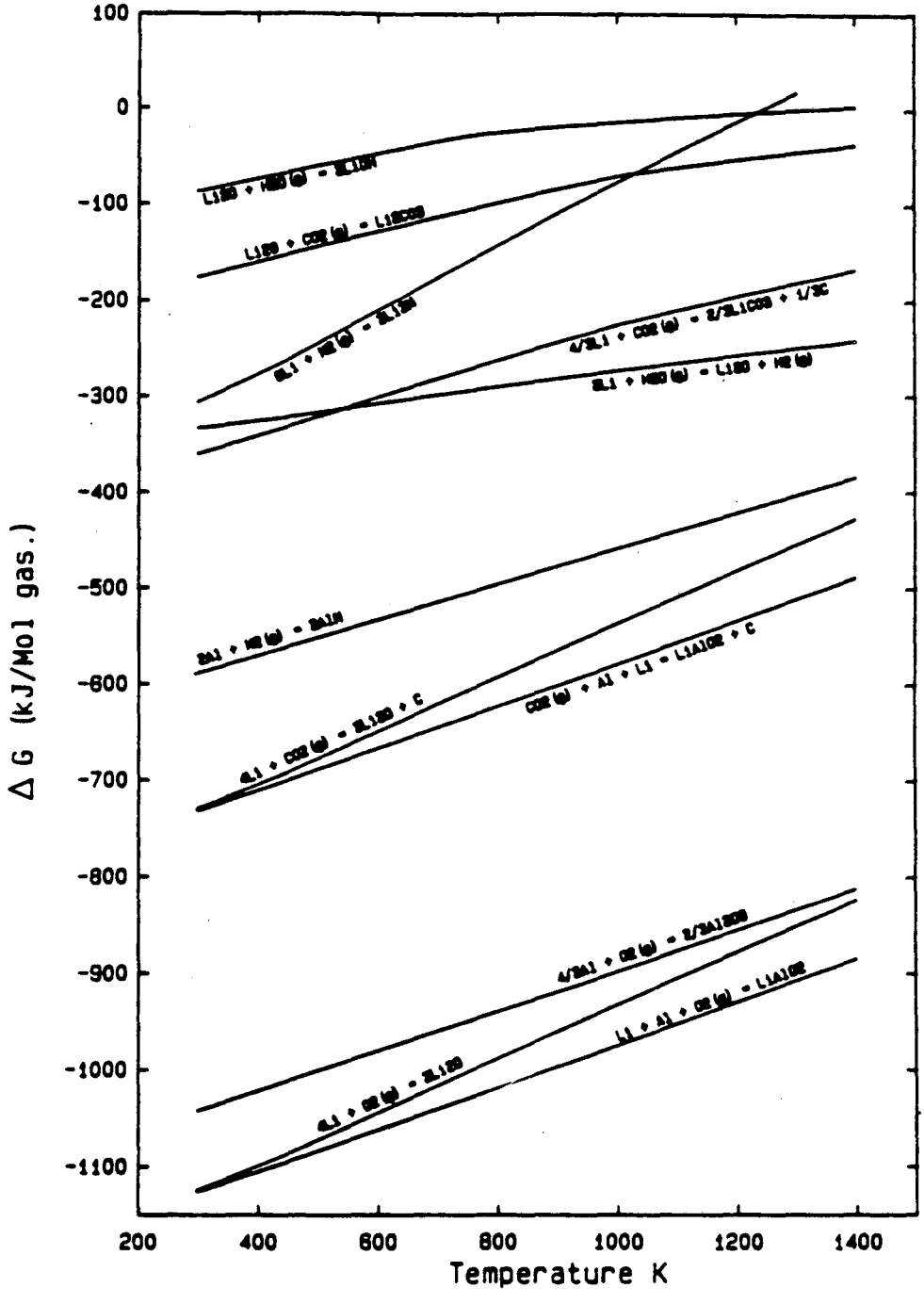

Fig. 2.2 Ellingham diagram for Al-Li alloy surface reactions

3. EXPERIMENTAL DESIGN AND SETUP

3.1 Design Considerations

There exists a large body of experimental as well as theoretical investigations concerning the solubility of gases in light metals. A literature review indicates that the basis for the determination of solubility of gases in these metals is Sievert's law, which essentially states that the amount of a gas dissolved in a metal or alloy is dependent on the pressure of the gas above the melt. For a diatomic gas X_2, which dissociates into atoms on dissolution

$$X_{2(gas)} \rightleftharpoons 2[X]_{(metal)}$$

The equilibrium for this reaction gives

$$K_e = \frac{[h_X]^2}{p_{X_2}}$$

Here, square brackets denote solution in metal phase and h_X denotes the Henrian activity. If the dissolved gas is sufficiently dilute to obey Henry's law, then

$$\text{wt\% } X = K_S \, p_{X_2}^{0.5}$$

where K_S is the Sievert's law constant.

Various experimental techniques are based on Sievert's law. Table 3.1 lists the techniques used by various investigators to determine the solubility of hydrogen in aluminum and its alloys. The alloys investigated do not include aluminum–lithium alloys.

TABLE 3.1

INVESTIGATOR	TECHNIQUE
1. W.R. Opie and N.J.Grant (3)	Sievert's apparatus using induction heating
2. Ransley and Newfield (4)	Sievert's apparatus using resistance heating
3. Ransley and Talbot (5)	Hot extraction method
4. Aschehoug et al (6)	Extraction and conversion of H_2 to H_2O
5. Brandt and Cochran (7)	Solid extraction Vacuum fusion
6. Ransley, Talbot and Barlow (8)	Pressure of H_2 entrained in a neutral gas circulating in the melt
7. Grigoreva and Danelkin (9)	Sievert's apparatus and Hardening Method
8. Degreve et al (10-12)	1. Vacuum extraction 2. Nitrogen carrier-fusion method 3. Quantitative vacuum gas test
9. Gee and Fray (13)	Electrochemical probe

The Sievert's technique essentially involves the measurement of the volume of gas absorbed by the metal or alloy being investigated.The extraction technique is based on the extraction of hydrogen and measuring it either directly or by conversion to water vapor.

On the basis of literature review and economic

considerations, the constant volume technique has been used to determine the solubility of gases in molten alloys. This technique was used in preference over the conventional techniques mentioned above owing to two reasons. The constant volume method has not been utilized for solubility determination and seems to be a alternative approach worth investigating. For the small solubilities involved, this method is thought to be more accurate and sensitive compared to other techniques.

In essence, this technique measures the pressure difference generated between a control volume subjected to an inert gas and an "active" volume subjected to the gas of interest, under identical conditions. The pressure difference generated is a measure of the solubility of the gas of interest in the alloy being investigated.

The experimental setup has been accordingly designed and the most important factors that had to be considered while designing the experimental setup were

(i) Temperature Range: Since this investigation has been primarily aimed at aluminum based alloys, the temperature range of interest has been taken from 650°C (10°C below the melting point of pure aluminum) to 750°C. This essentially covers the range of casting temperatures of these alloys.

(ii) Volume Considerations: It has been estimated that the solubility of hydrogen in aluminum lithium alloys should be in the range of 0.5 - 5 ppm. With this and using 5 grams of the

sample as the basis, we can generate the following table. [Details of the calculations involved are shown in Appendix I]. This table gives the pressure difference generated, ΔP, as a function of gas volume for $T=1000^{o}K$.

TABLE 3.2

Effective Volume (cm^3)	ΔP @ 0.5 ppm (mm Hg)	ΔP @ 5 ppm (mm Hg)
30	2.58	25.79
40	1.93	19.34
50	1.55	15.47
60	1.29	12.88
70	1.10	11.05

It is evident from the above table that as the volume is increased, the pressure difference generated due to gas solubility will decrease. To ensure meaningful and reproducible data, one of the most important design criteria is to keep the effective volume of the setup as small as possible. However, reducing the volume too much poses fabrication problems and a compromise was established at 50 cm^3.

Based on the above criteria, the experimental setup has been designed. Other important factors were

(i) Stability of temperature: solubility is a function of temperature and consequently it is essential to avoid temperature

gradients in the heating environment. This was one of the criteria used in the selection of the furnace.

(ii) Precision of pressure measurement devices: As shown in Table 3.1, the estimated pressure drops are small and the devices to measure these have to be sensitive to small changes in pressure.

(iii) Containment of the alloy: The alloy has to be housed in a material that is inert to the gases being used and this material should not evolve gases on heating leading to spurious results.

(iv) Minimization of the "dead volume": In the experimental setup, the dead volume (the volume of the setup that is in the non-isothermal zone) has to be kept to a minimum so as to avoid errors in the pressure drop due to temperature gradients in this region. An expression for the contribution in the pressure drop due to the dead volume has been derived and is shown in Appendix II. This expression has been shown to be satisfactory as a first approximation.

3.2 Experimental Setup

On the basis of the design considerations described earlier, the experimental apparatus was constructed. A schematic of the experimental apparatus is shown in Fig. 3.1 and a photograph is shown in Fig. 3.2.

The heart of the setup is a three zone vertical gold plated furnace made of two concentric quartz tubes. The inner tube has a 65mm inner diameter (ID) and a 70mm outer diameter (OD). The

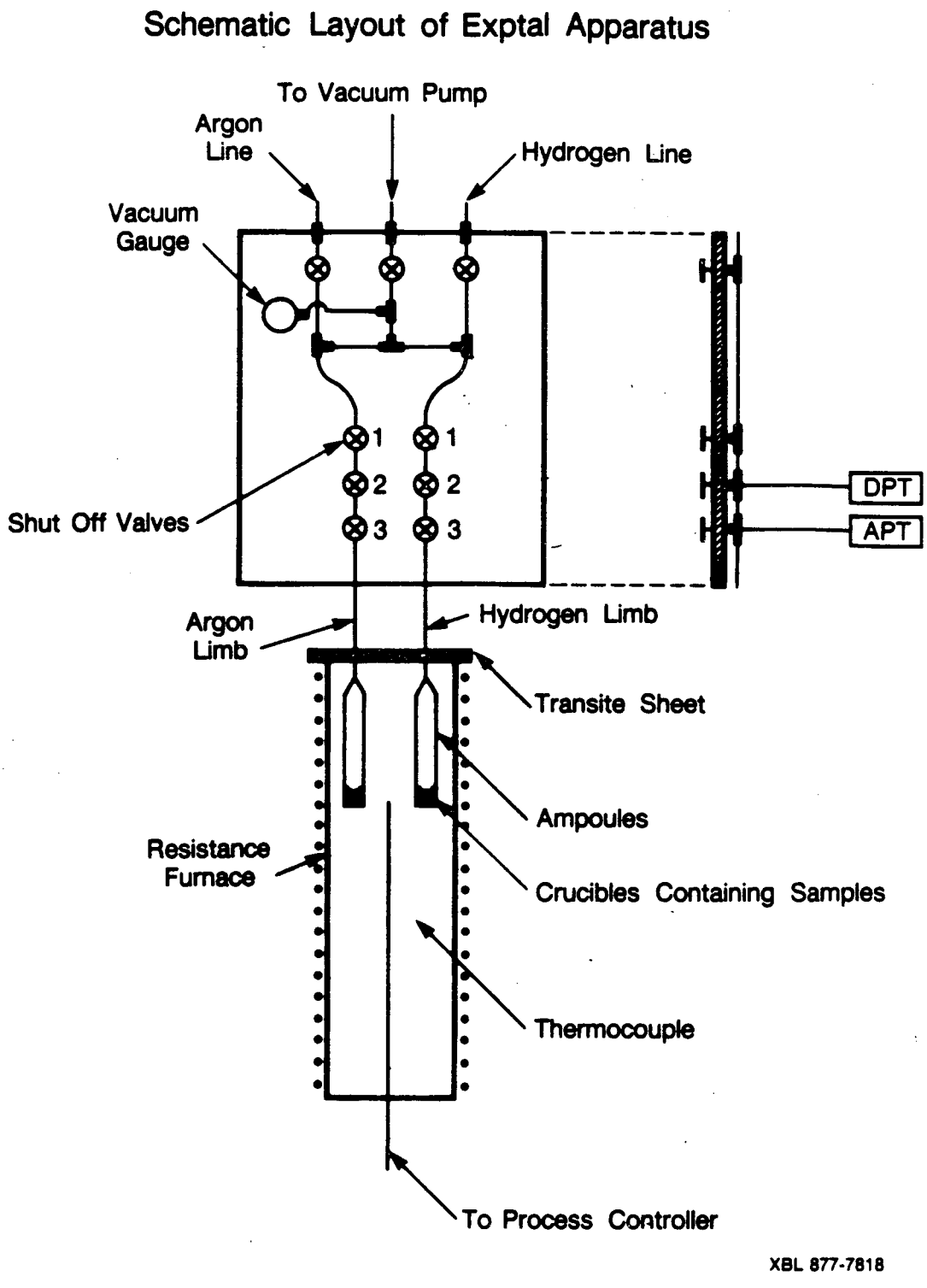

Fig. 3.1 Schematic layout of experimental setup

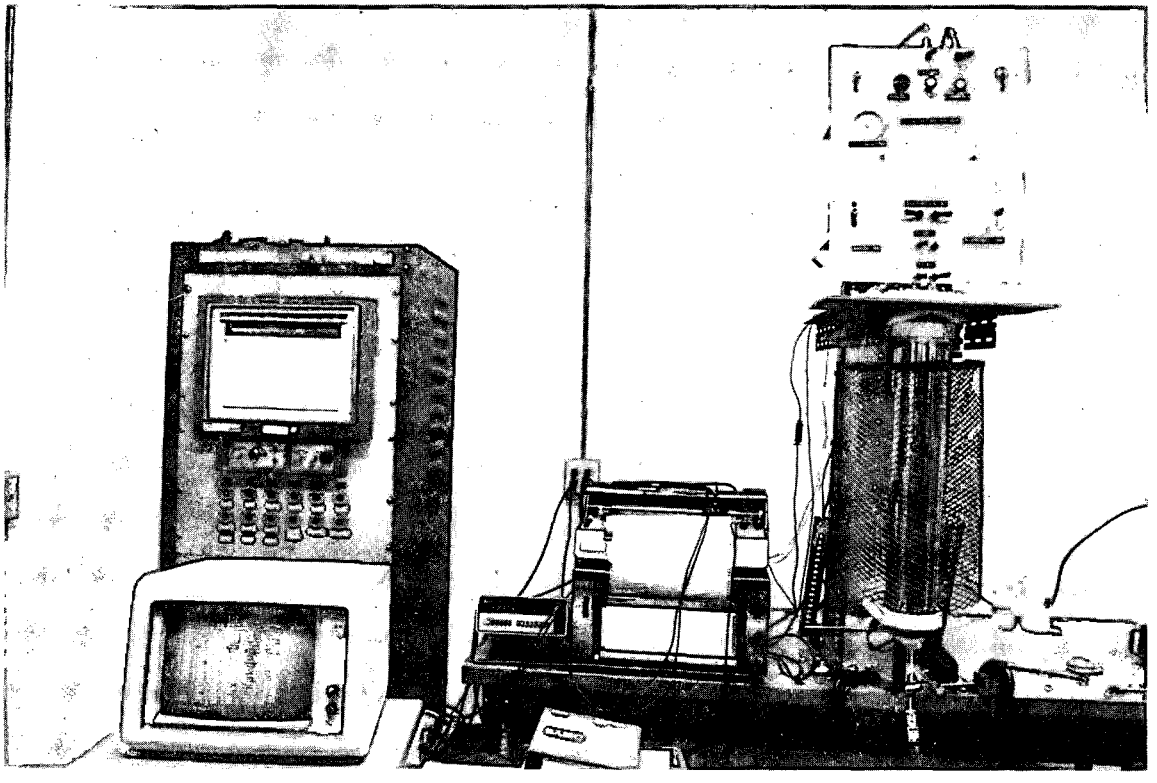

XBB 878-6671

Fig. 3.2

outer tube has a 80mm ID and 85mm OD and the height of the furnace is 610mm. The heating element is housed between the quartz tubes and is made up of three zones. There is a central heating coil and guard coils on the ends which provide a uniform temperature gradient through the length of the furnace. In the trial runs, the temperature remained uniform with a variation of $\pm$ 1^{o}C, except for 5 cms at the ends. This uniformity in temperature is further aided by the fact that the outer tube is gold plated. Gold is transparent to visible radiation and blocks out infra-red radiation, leading to thermal uniformity. It also enables us to look inside the furnace at temperatures above 600^{o}C. The furnace was supplied by Trans Temp Co., Chelsea, MA.

The furnace is mounted vertically, and the ends are insulated with Fibrefax and a protective wire mesh surrounds it to prevent accidental collisions.

Inside this furnace sit two identical quartz ampoules of 22mm ID and 24mm OD and 158-160mm height. These ampoules house the crucibles containing the alloy. The dimensions of the crucible are 18mm ID and 30mm height and the crucibles, made of alumina, have been supplied by Technical Distributors Inc., San Jose, CA. The ampoules are connected via quartz tubing of 4mm ID and 6mm OD to a graded quartz to pyrex seal onto a Cajon pyrex to stainless steel seal. The stainless steel end of the seal fits into a Swagelok fitting which is further connected to the gas supply lines and the vacuum line.

All the tubing external to the furnace is made of 316 stainless steel and there are separate lines for argon, hydrogen and the vacuum pump. A vacuum gauge is connected to the vacuum line. The gas supply and vacuum lines are regulated by Nupro valves. All of the tubing is housed in a modular arrangement which has three degrees of movement. Variations in ampoule orientation due to glassblowing can thus be accommodated during placement inside the furnace. This module was leak tested and found to be leak tight.

An absolute pressure transducer (APT) is connected to one limb of the setup in which argon is contained (hereafter referred to as the argon limb), and a differential pressure transducer (DPT) is connected across the argon limb and the other limb in which hydrogen is usually contained (hereafter referred to as the hydrogen limb). Both of these transducers are of the capacitive type and were supplied by Setra Systems, Nagog Park, Acton, MA. The APT is a model 280E with a range of 0 to 25 psia (0 - 1300mm Hg) and the DPT is a model 239 with a bidirectional range of 0 $\pm$ 2.5 psi (0 $\pm$ 130mm Hg). The reference port of the DPT is connected to the hydrogen limb and the positive pressure port is connected to the argon limb. Both transducers are connected to Setra model 300E digital pressure meters which convert the electrical signals from the transducers into pressure readings in units of mm Hg. The DPT can give both positive and negative readings and a negative reading implies that the pressure in the

hydrogen limb is greater than the pressure in the argon limb and vice versa.

The temperature is measured using a K-type (chromel-alumel) thermocouple placed between the ampoules at the bottom of the furnace. Its output is connected to a Research Inc. model 6400 process controller which controls the temperature of the furnace. The thermocouples used were tested in various environments and were found to be accurate enough for this investigation (details in section 3.5).

The APT and the thermocouple are connected to strip chart recorders and the DPT and APT outputs have been interfaced with an IBM PC-XT to continuously collect the data and to assess whether the system has attained equilibrium.

The setup was initially fabricated using glass valves and glass tubing. However, they had to be replaced by stainless steel valves and tubing because the glass fittings were fragile and liable to break, and were not leakproof. Considerable time and effort were devoted to the initial setup but it proved to be a futile effort and the setup had to be refabricated.

3.3 Modus Operandus

The basic idea of this technique is to measure the pressure difference between a control and an active volume. A two-part experimental scheme was evolved based on design considerations already discussed and experience gained from earlier experiments, and a typical run is described below. The first part uses argon

in both limbs of the apparatus and the second part uses argon in the argon limb and hydrogen in the hydrogen limb. In certain runs, Part II was repeated to ensure reproducibility, and Table 4.2 describes these runs in detail.

To begin with, the alloy, which is generally in the form of a slab or a lump, is cut into small cubes of approximate dimensions 4-5mm on each side. The alloy (2090 Al-Li alloy supplied by Kaiser Aluminum Co., Pleasanton, CA) is then washed with acetone to remove surface organic contaminants, and dried. Equal amounts of the alloy are weighed out, usually 5-7 grams, and placed in alumina crucibles. The samples are weighed up to the fourth decimal place and the weights differ by not more than 0.01 gms. Care is taken to avoid contamination by touching.

Each crucible is loaded in an ampoule which is sealed by glass-blowing. In the process, water vapor is formed inside the ampoule which may cause formation of surface oxides and hydrides, leading to incorrect results. To eliminate water vapor, the ampoules are connected to the setup through Swagelok fittings and the furnace is brought up to a temperature of 150-175^{o}C. The vacuum pump is switched on and the system is evacuated at this temperature for 8-10 hours, at the end of which the water vapor is eliminated and the setup is cooled to ambient temperature.

Part I: At this point, the argon line is opened and both

ampoules are filled up with argon to a predetermined pressure (usually 100, 225 or 350 mm Hg) and the shutoff valves to the argon and hydrogen limbs are closed, isolating the two limbs. The only connection between the two limbs is the DPT. The APT is connected to the argon limb and monitors absolute pressure. The furnace is again switched on and the temperature is increased using the analog process controller. Set points 0-100-150-200-250-300 correspond to ambient temperature-270-390-510-625-742°C. At each set point, the system is allowed to equilibrate and temperature, absolute pressure and differential pressure are noted. Equilibrium is considered to be established when temperature and absolute pressure do not vary significantly with time.

Part II: The furnace is switched off, the vacuum pump is switched on, the shutoff valves are opened and the system is allowed to cool to ambient temperature.

Now the argon limb is opened, the hydrogen limb is closed and the argon limb is filled to the previous predetermined pressure. Then the argon limb is closed, the hydrogen limb is opened and is filled to an equal pressure (determined using the DPT) with hydrogen. The furnace is then switched on again, and the heating cycle is repeated. The temperature is then increased slightly (by 15-20°C) and the vacuum line is opened to evacuate the system of dissolved hydrogen. Then the system is allowed to cool down.

A typical experiment (either Part I or II) would take about 4-5 hours to heat up and equilibrate and 3-4 hours to cool to ambient temperature, making the total experimental time 8-10 hours.

3.4 Analysis of Experimental Data

Data from Parts I and II are plotted as absolute and differential pressure versus temperature. The differential pressure versus temperature graph shows Part II curves (argon and hydrogen) to lie above Part I curves (argon and argon), indicating a pressure drop due to hydrogen solubility in the alloy. This difference, ΔP, in the differential pressures of Parts I and II, is the pressure drop due to hydrogen solubility and to non-ideality of the gases and any volume differences that may exist between the ampoules. This ΔP is then corrected to account for these variations (details of these corrections are in Chapter 4).

Knowing the volume of the experimental setup (approximately 50 cm^3) and the temperature, the number of moles of hydrogen dissolved is calculated using ideal gas laws. The exact volume of the setup is determined by measurement after the experiments are over using water injected into the ampoules from a precision syringe.

With the mass of the sample and number of moles of dissolved hydrogen known, solubility is expressed as parts per million

(ppm). Details of calculations for a typical set of experimental data are shown in Appendix III.

3.5 Experimental Program

The preliminary work included:

(i) Calibration of the furnace in order to establish its temperature profile, and calibration of the process controller.

(ii) Calibration of thermocouples using ice water, boiling water and a furnace of known temperature behavior. Thermocouple placement in the furnace was checked to establish variance in recorded temperature, which in our case was zero except at the ends.

(iii) Calibration of pressure meters to verify accuracy and sensitivity. This was done by applying known voltages across them and comparing the output with those supplied by the manufacturer.

Some time was then spent on developing the modus operandus of the experiment, as described in section 3.4. An overall experimental program was then designed which consisted of the following stages:

Stage 1: The objective of this stage was two-fold; first, to compare theoretical and observed values of the pressure, i.e. to establish the effect of the dead volume, and second, to identify and evaluate factors other than hydrogen solubility that might contribute to ΔP. In the first part, observed absolute pressures were compared with theoretical pressures calculated

from expression A3 (refer Appendix II). The effect of dead volume was established and a certain degree of confidence in the experimental set-up was gained.

In the second part, the factors considered were the effect of crucibles, the different natures of the gases involved, and variations in ampoule volumes due to glass-blowing. To evaluate the effect of crucibles, ampoules were loaded with empty crucibles and pressure data collected under various experimental conditions. To establish the effect of the different nature of gases and variation in ampoule volumes, runs were made with empty ampoules (no crucibles), with argon in the argon limb and hydrogen in the hydrogen limb, for various initial pressures.

Stage 2: The preceding experiments gave a fair indication of the accuracy and limitations of the experimental set-up, and experiments were then conducted to establish the solubility of hydrogen in aluminum–lithium alloys.

4. EXPERIMENTAL RESULTS AND DISCUSSION

4.1 Effect of dead volume

The effect of the dead volume has been assessed by comparing the observed absolute pressures with the calculated pressures from expression A3 derived in Appendix II. The absolute pressures from experiments ALI350Ar1 and ALI350Ar2 (refer Table 4.2) are plotted in Fig 4.1 and are compared with the calculated pressures. In expression A3, the experimental volume is considered to be made up of two parts – a bulk volume, V_b, at the experimental temperature and a dead volume, V_d, at ambient temperature and calculations are done accordingly. The observed pressures are shown as dashed lines and the calculated pressures are shown as solid lines. There is excellent agreement with experimental observations. This leads to a greater degree of confidence in the ability of our experimental apparatus to yield meaningful results.

As the basis of these experiments is measurement of a differential pressure, it was important to identify factors other than hydrogen solubility which might contribute to it, and the following experiments were carried out in order to evaluate these factors.

4.2 Effect of crucibles

These experiments were performed in order to assess whether the crucibles themselves might contribute to the differential

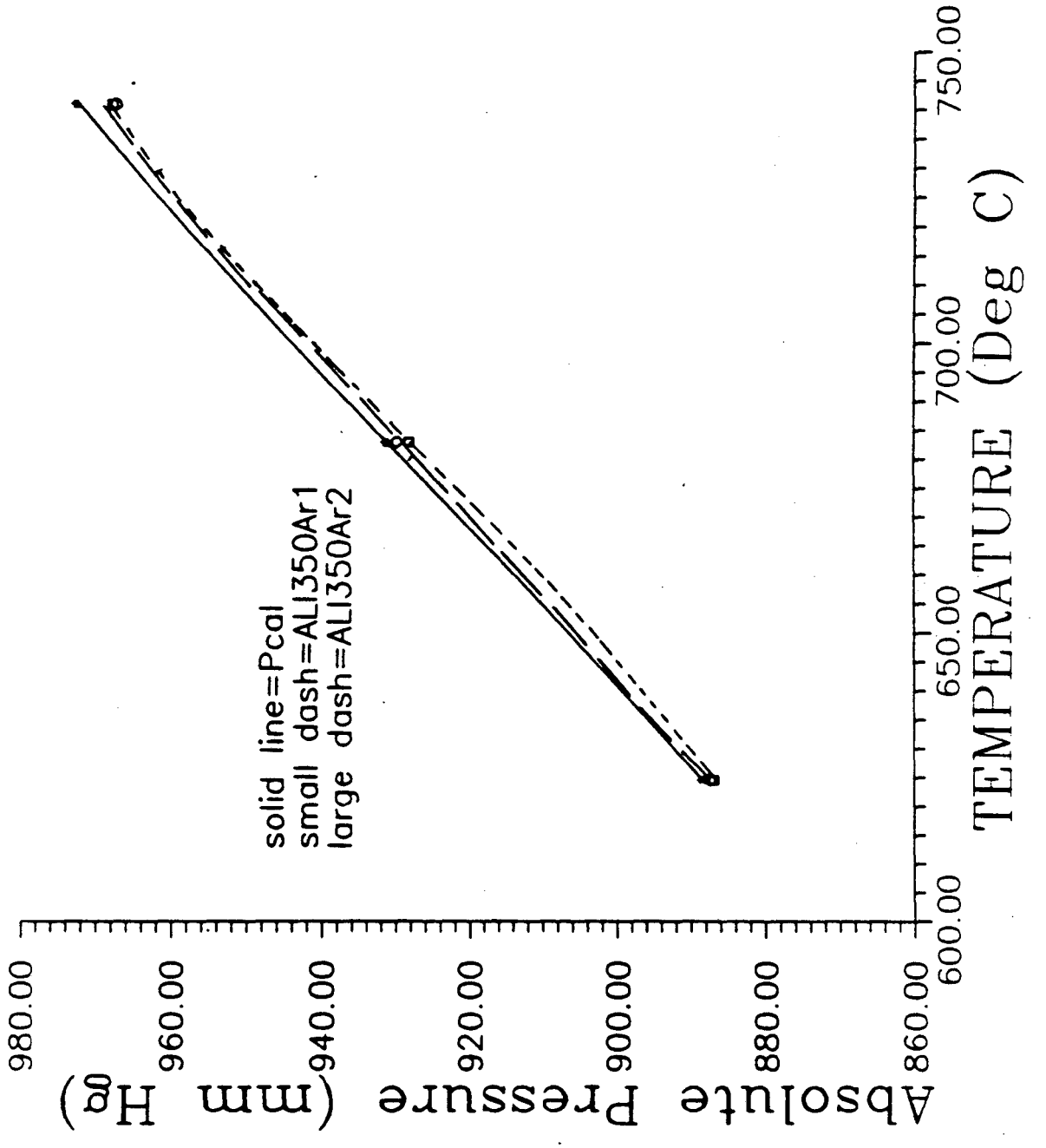

Fig. 4.1 Absolute pressure for ampoules filled with argon

pressure by absorbing or desorbing gases or water vapor. Runs were made using empty crucibles sealed into ampoules. Experimental conditions for the various runs are shown in Table 4.1.

Table 4.1

Experiments and experimental conditions for determining effect of crucibles

EXPT #	EXPERIMENTAL CONDITIONS		
	Gas used	Initial values of P_{abs}	P_{diff}
AMAR1	Ar in both limbs	300 mm	-13.89mm
AMAR2	Ar in both limbs repeat of AMAR1	300.8mm	−13.50mm
AMAR3	Ar in both limbs Ampoules exposed to air for 24 hrs prior to experiment	299.6mm	−13.12mm
AMH21	Ar in Ar−limb H_2 in H_2−limb	293.1mm	−13.00mm
AMH22	repeat of AMH21	297.6mm	-12.87mm
AMH23	repeat AMH21 after evacuation done at 750°C	302.2mm	−14.08mm
AMH24	Ampoules exposed to air for 48hrs repeat AMH21	303.8mm	−13.00mm
AMH25	repeat AMH21 after resealing crucibles in ampoules	307.2mm	−13.00mm

The results from the above experiments are shown in Figs 4.2–4.5. Fig 4.2 shows the variation of absolute pressure with temperature for the AMAR series of experiments (those with argon in both ampoules). Fig 4.3 shows the variation of the differential pressure with temperature for the AMAR series of experiments. The various experimental conditions do not significantly affect the absolute pressure. In Fig 4.3, there is a significant difference between AMAR1 and AMAR2. No evacuation was done in between these runs and that seems to be a probable cause for the observed discrepancy. As seen in the subsequent experiments, evacuation at elevated temperatures seems to be a solution. Figs. 4.4 and 4.5 show the variation in absolute and differential pressures for the AMH2 series of experiments (those with argon in the argon–limb and hydrogen in the hydrogen–limb). Evacuation at elevated temperatures results in experimental reproducibility as can be seen in Fig. 4.5 where after expt AMH22 there is an evacuation step at 750°C. Subsequent experiments, AMH23 to AMH25 show reasonable reproducibility. Evacuation at elevated temperatures seems to be a very important step to ensure reproducibility and has been done in all subsequent experiments. Other factors like exposure to atmosphere and water vapor which can occur during experiments, do not appreciably alter pressure variations. It may therefore be concluded that the crucibles will not appreciably contribute to ΔP, if they have been evacuated at elevated temperatures.

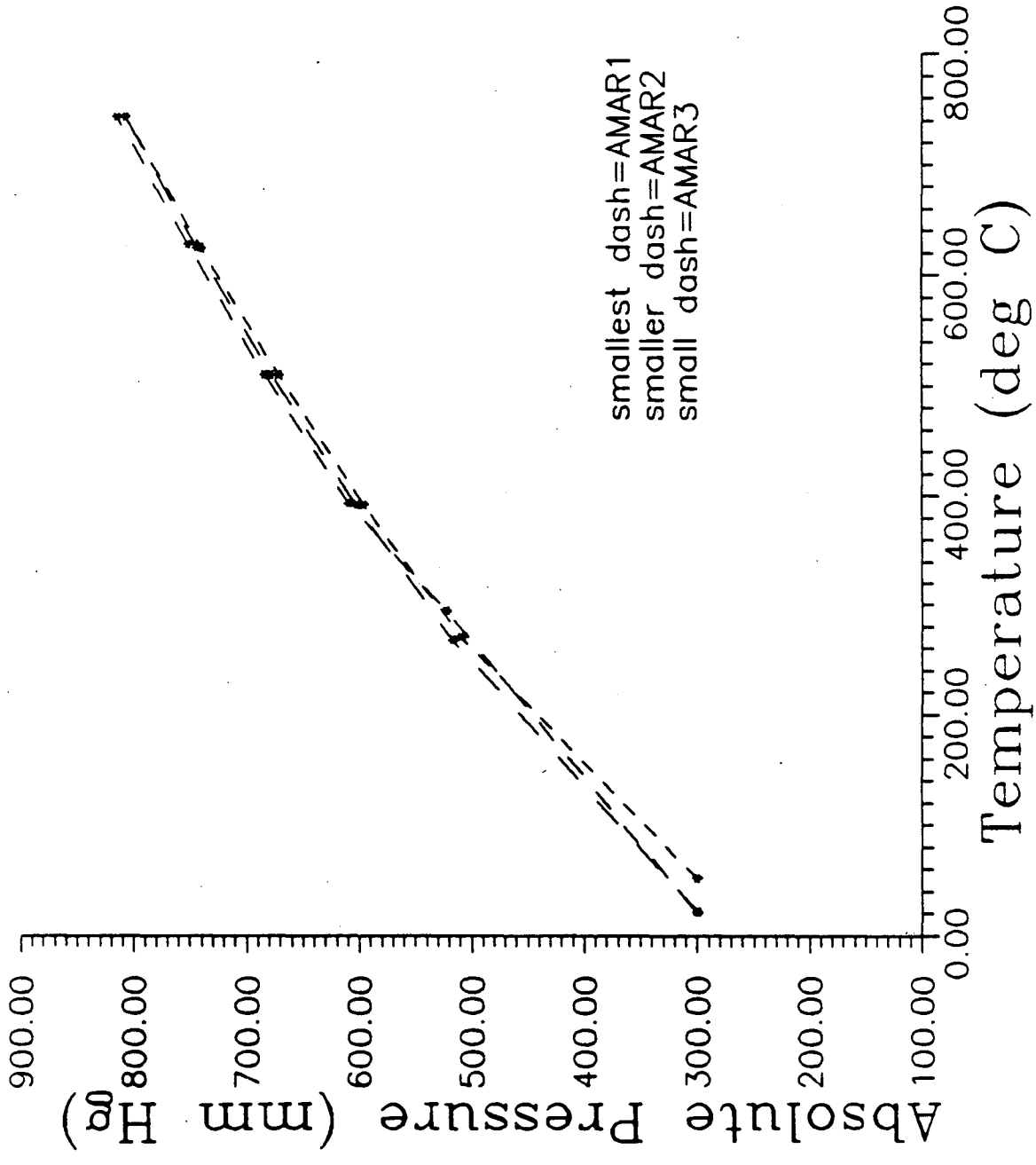

Fig. 4.2 Absolute pressure for ampoules with blank crucibles with Ar in both limbs

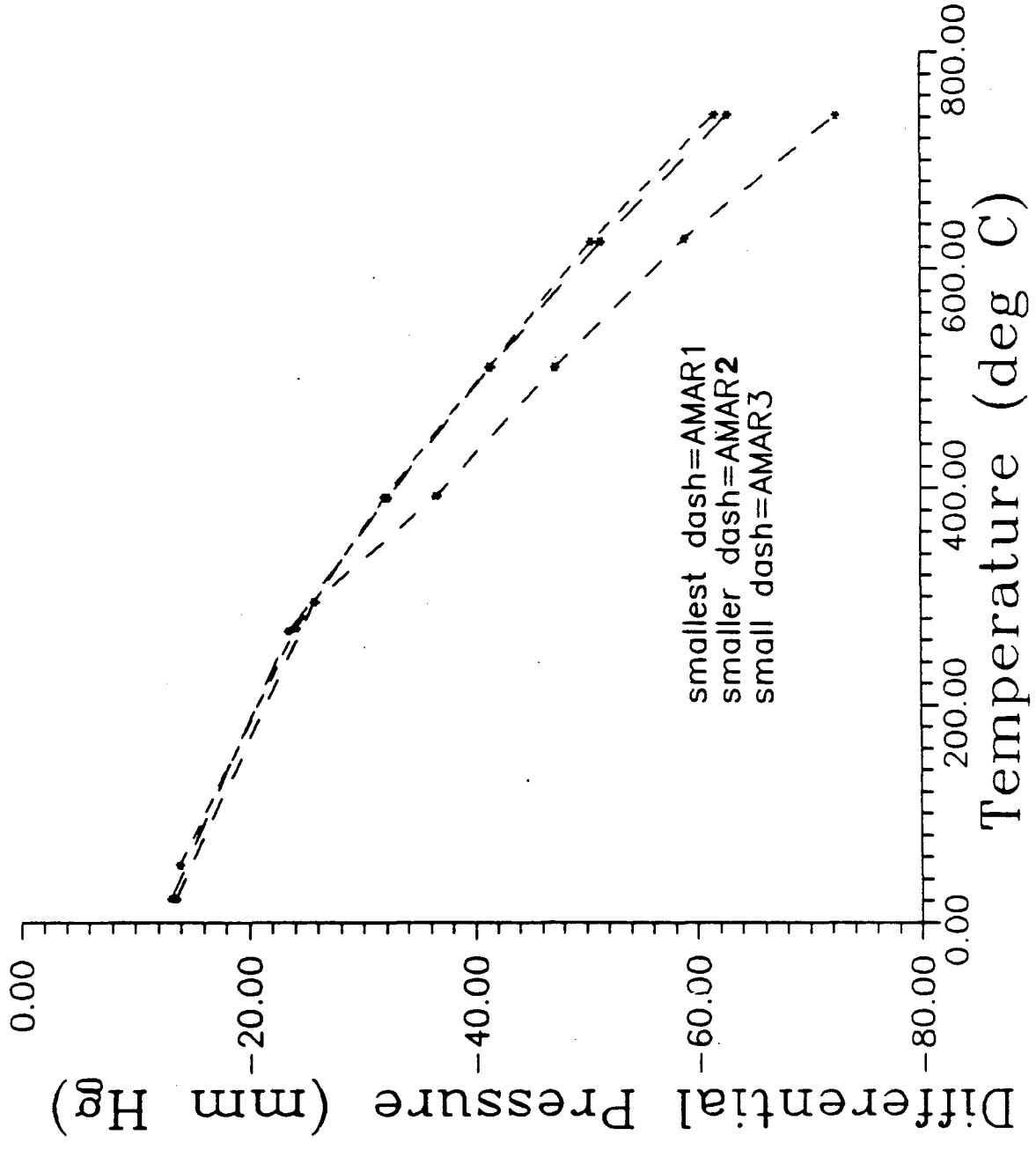

Fig. 4.3 Differential pressure for ampoules with blank crucibles with Ar in both limbs

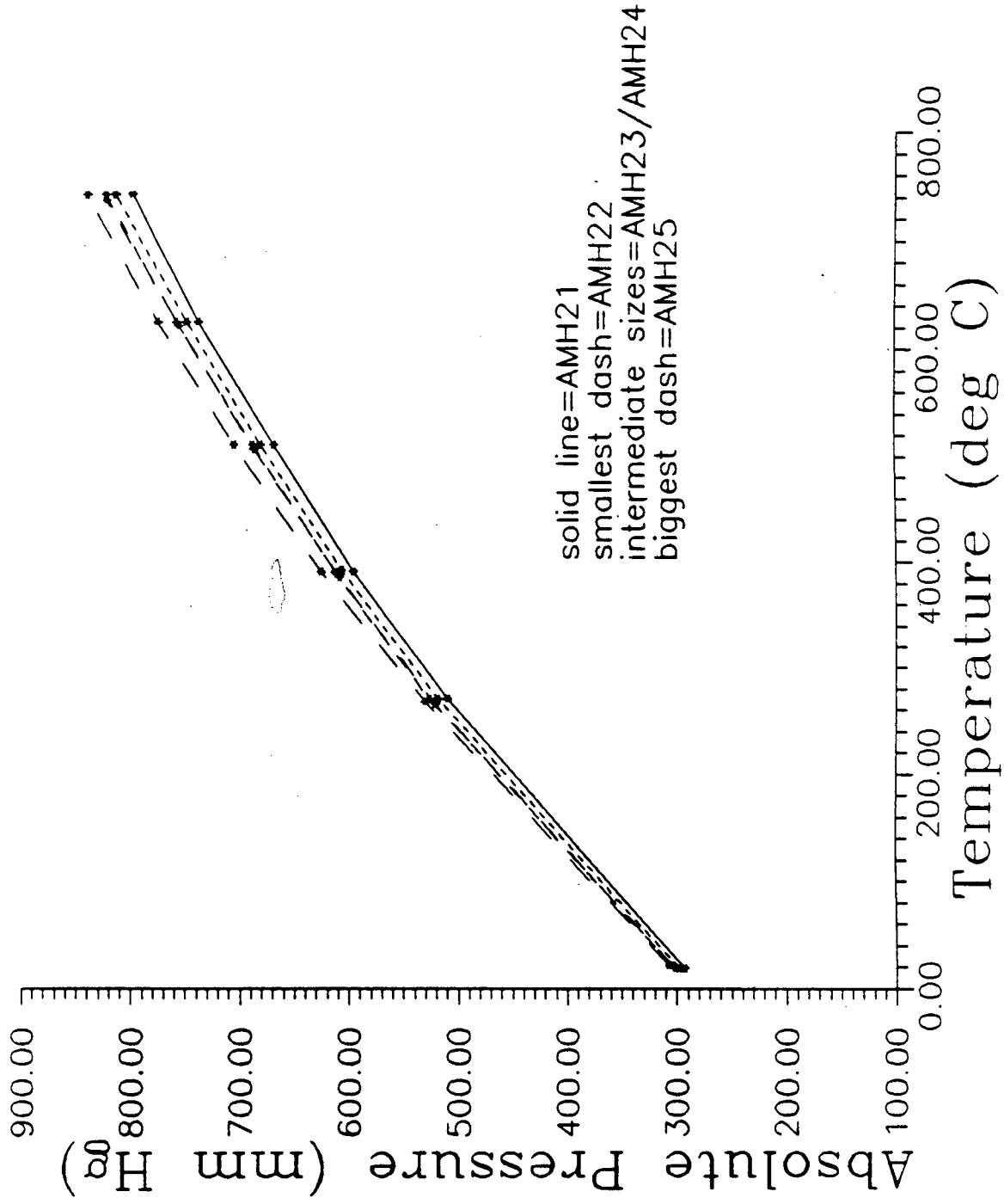

Fig. 4.4 Absolute pressure for ampoules with blank crucibles with Ar in Ar-limb and H_2 in H_2-limb

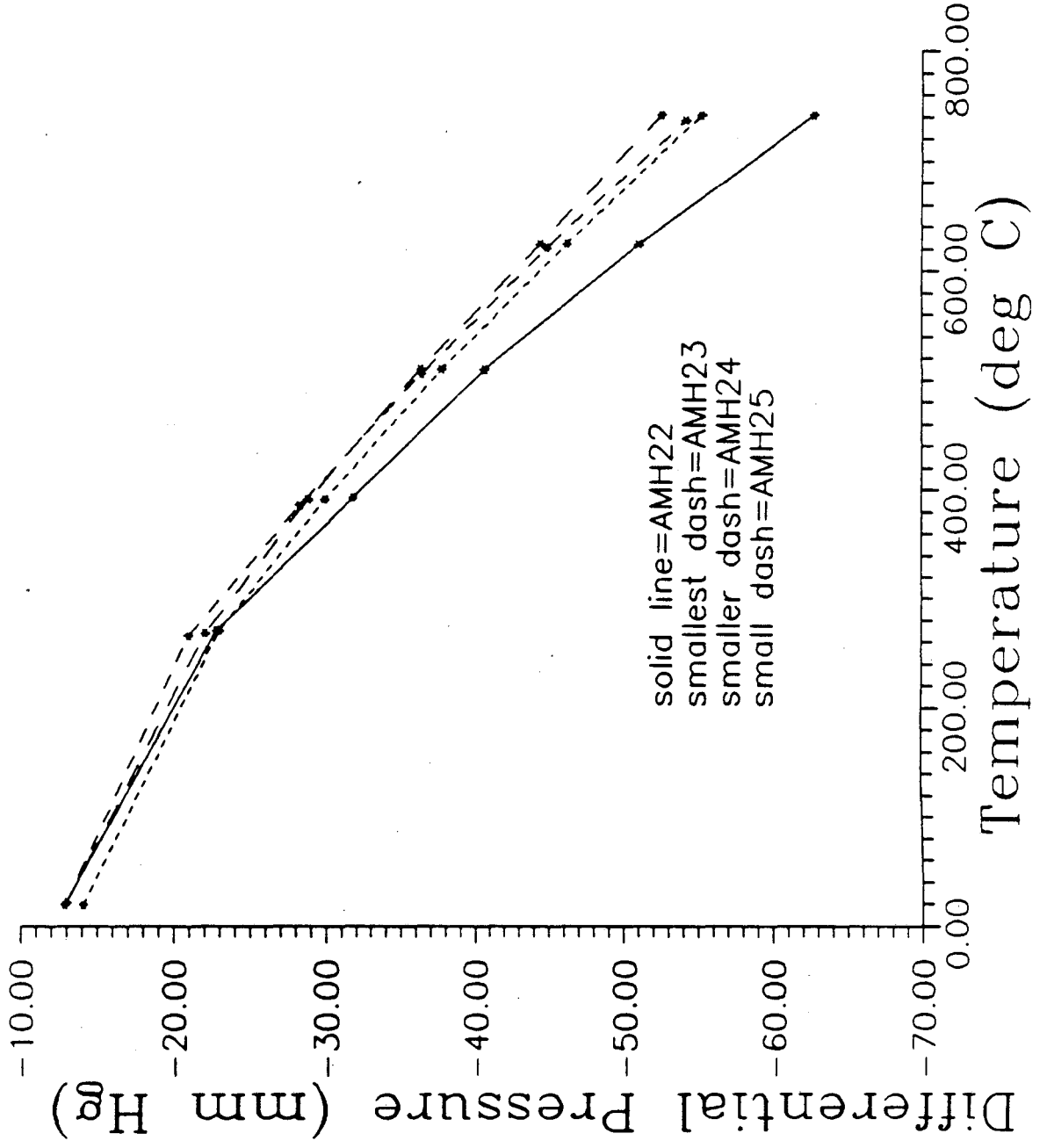

Fig. 4.5 Differential pressure for ampoules with blank crucibles with Ar in Ar-limb and H_2 in H_2-limb

4.3 Effect of gases

To assess the effect of having different gases in the different limbs, runs were made with empty ampoules (no crucibles). Experiments were carried out as described in Chapter 3.4 for initial pressures of 100, 225 and 350 mm Hg. The differences (ΔP) in the differential pressures between Part I and Part II experiments are shown in Fig 4.6 for the various initial pressures. There seems to be a significant ΔP for the 350 and 225 mm runs. This ΔP is not only due to the nonideal behavior of argon and hydrogen, but may be also due to variations in ampoule volumes due to glassblowing, and thermal expansion of quartz.

This ΔP is used as a correction term for subsequent experiments. For the 100 mm run with empty ampoules, the difference was between 1 and 2 mm Hg. This could be due to thermal fluctuations owing to limitations of the process controller The ΔP for the 100 mm run has therefore not been shown in Fig. 4.6 and a standard correction of 1.5 mm in ΔP for all temperatures has been used in calculations for runs made at 100 mm.

The experiments and results discussed above essentially validate the efficacy and shortcomings of the experimental technique.

4.4 Experiments with aluminum lithium alloys (2090 series)

Table 4.2 below describes experiments performed using aluminum lithium alloys at various initial pressures.

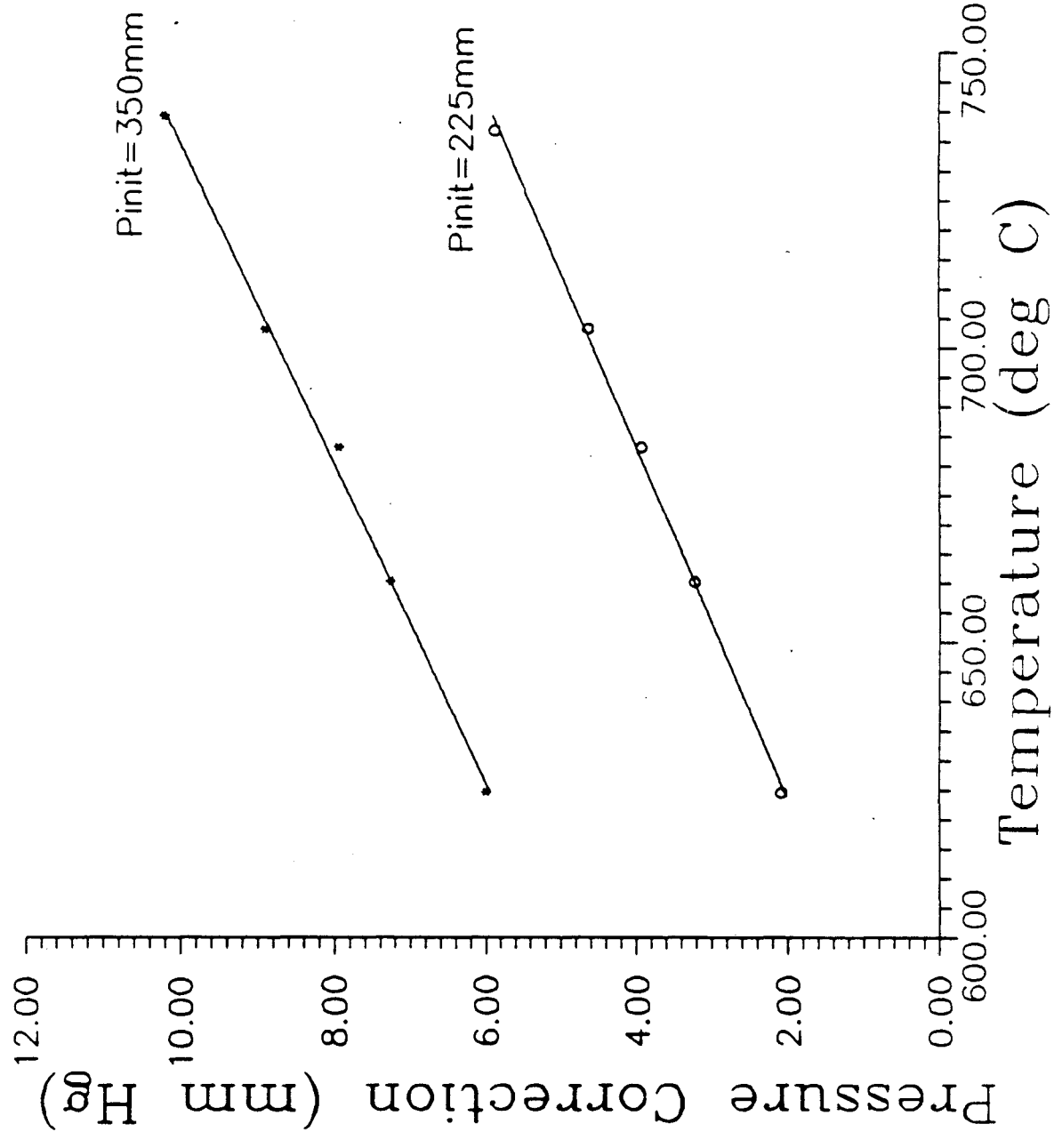

4.6 **Pressure correction due to difference in differential pressures between Ar-Ar and Ar-H_2 runs with empty ampoules**

TABLE 4.2

EXPT.	Evacuation time at 660 C prior to experiment	Gas combination	Initial P_{abs} mm	Initial P_{diff} mm
ALI350Ar1	20 min	Ar-Ar	351	-13.70
ALI350Ar2	20	Ar-Ar	351	-13.68
ALI350H1	20	Ar-H_2	349.4	-13.96
ALI350H2	20	Ar-H_2	350.5	-14.05
ALI350H3	30	Ar-H_2	349.9	-14.05
ALI350H4	20	Ar-H_2	349.2	-14.00
ALI225H1	20	Ar-H_2	224.8	-13.86
ALI225Ar1	20	Ar-Ar	224.8	-13.71
ALI100Ar1	20	Ar-Ar	100.4	-13.86
ALI100H1	20	Ar-H_2	100.4	-13.71

The results of these experiments are shown in Figs. 4.7-4.11. Fig. 4.7a – 4.7c show the variation in differential pressure for the ALI series of experiments for initial pressures of 100, 225 and 350 mm Hg. In Fig. 4.7a, a fair degree of reproducibility was obtained for the various experimental conditions described above. In fact, for the experiment ALI350H4 the full circle represents a data point that was obtained on cooling from the higher temperature. This data point falls on the curve drawn and implies that there is some sort of equilibrium achieved. Fig. 4.8 shows variation in absolute pressure for initial pressures of 100 to 350 mm. Fig. 4.9 shows differences in differential pressures (ΔP) corrected for variations in ampoule volume, non-ideality of gases used, and thermal expansion of quartz. (To ensure uniformity, data from Figs. 4.6 – 4.8, which range from 620°C to

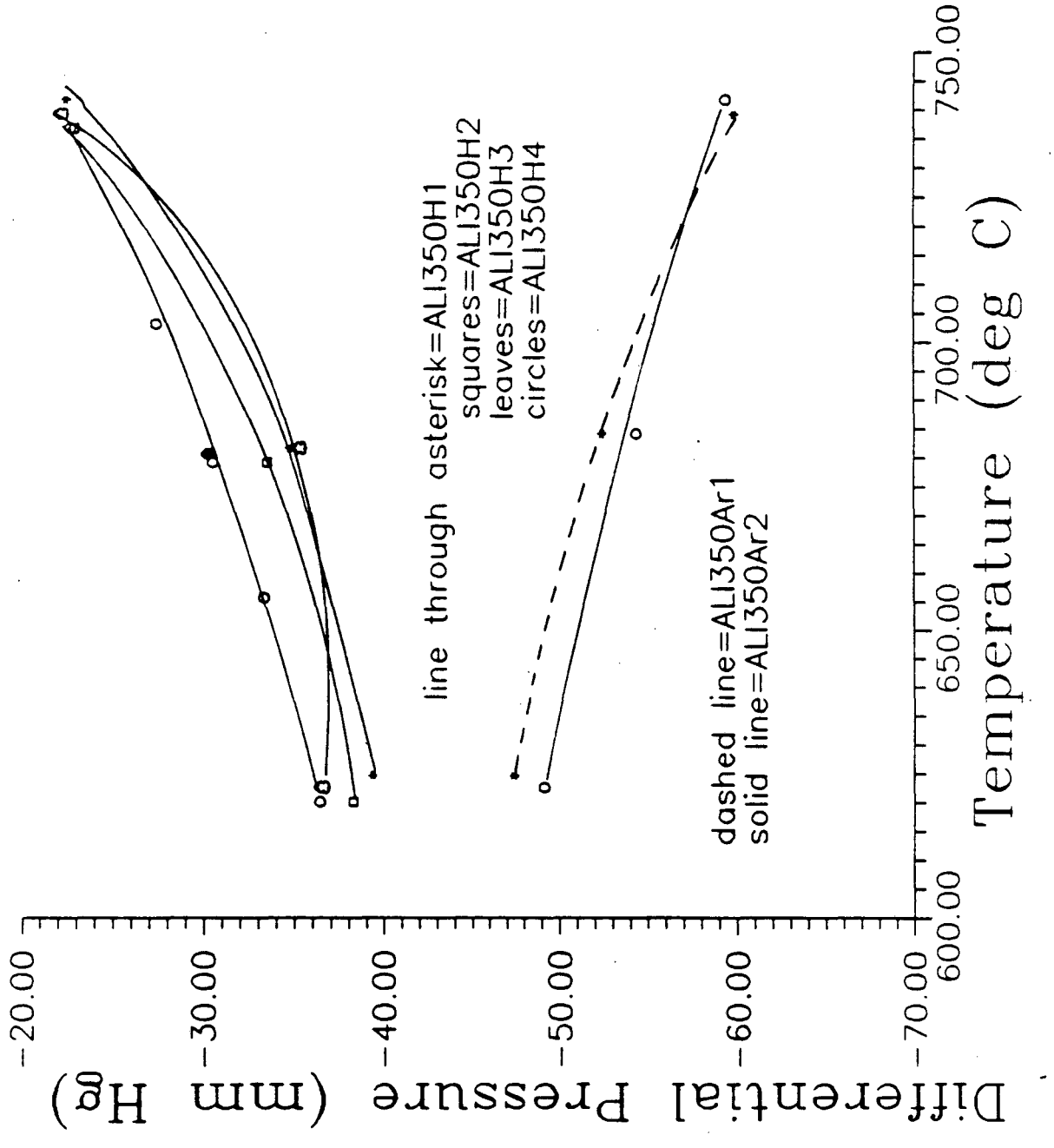

Fig. 4.7a Differential pressure for ampoules containing Al-Li alloy at P_{init} = 350 mm Hg

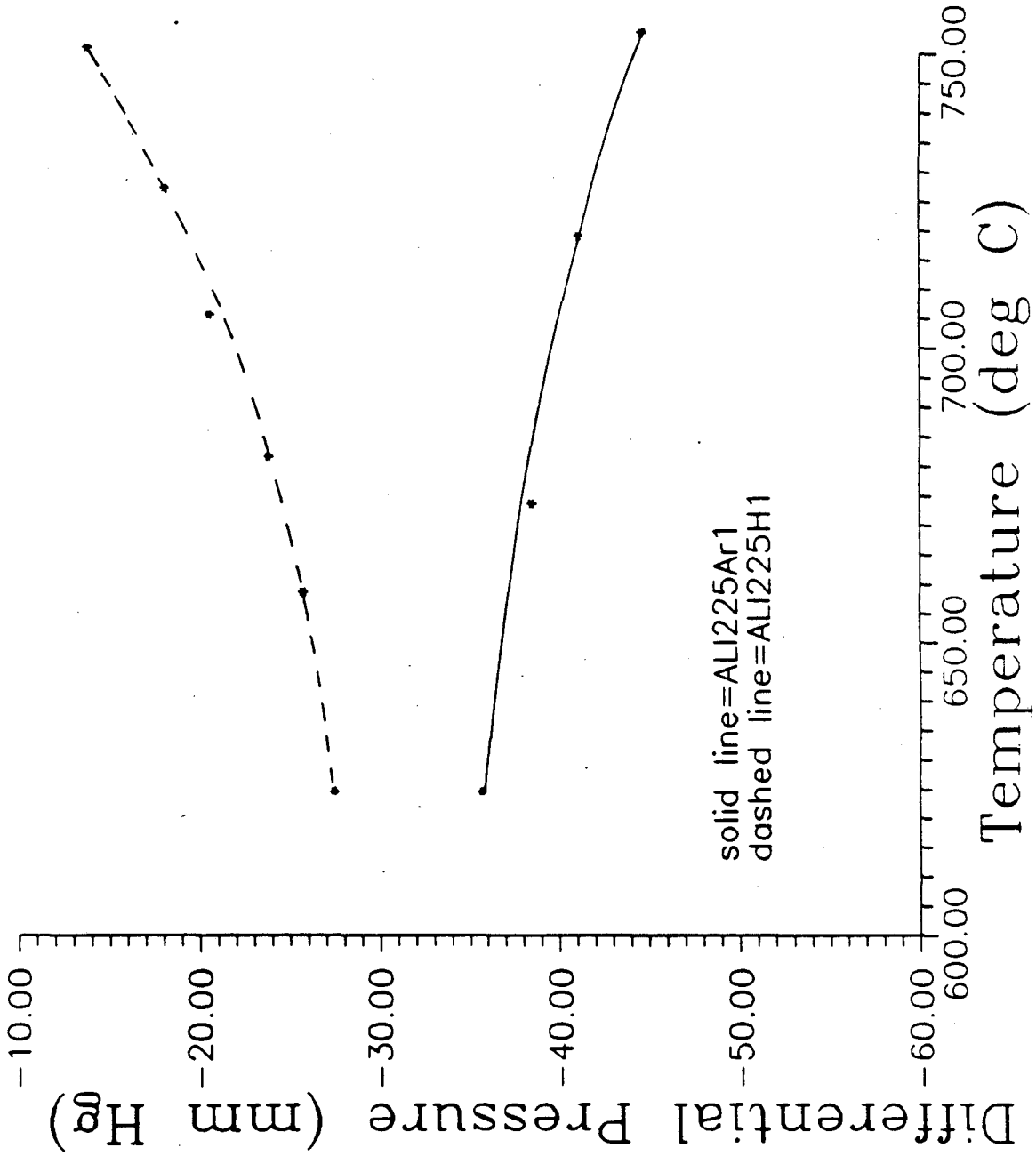

Fig. 4.7b Differential pressure for ampoules containing Al-Li alloy at P_{init} = 225 mm Hg

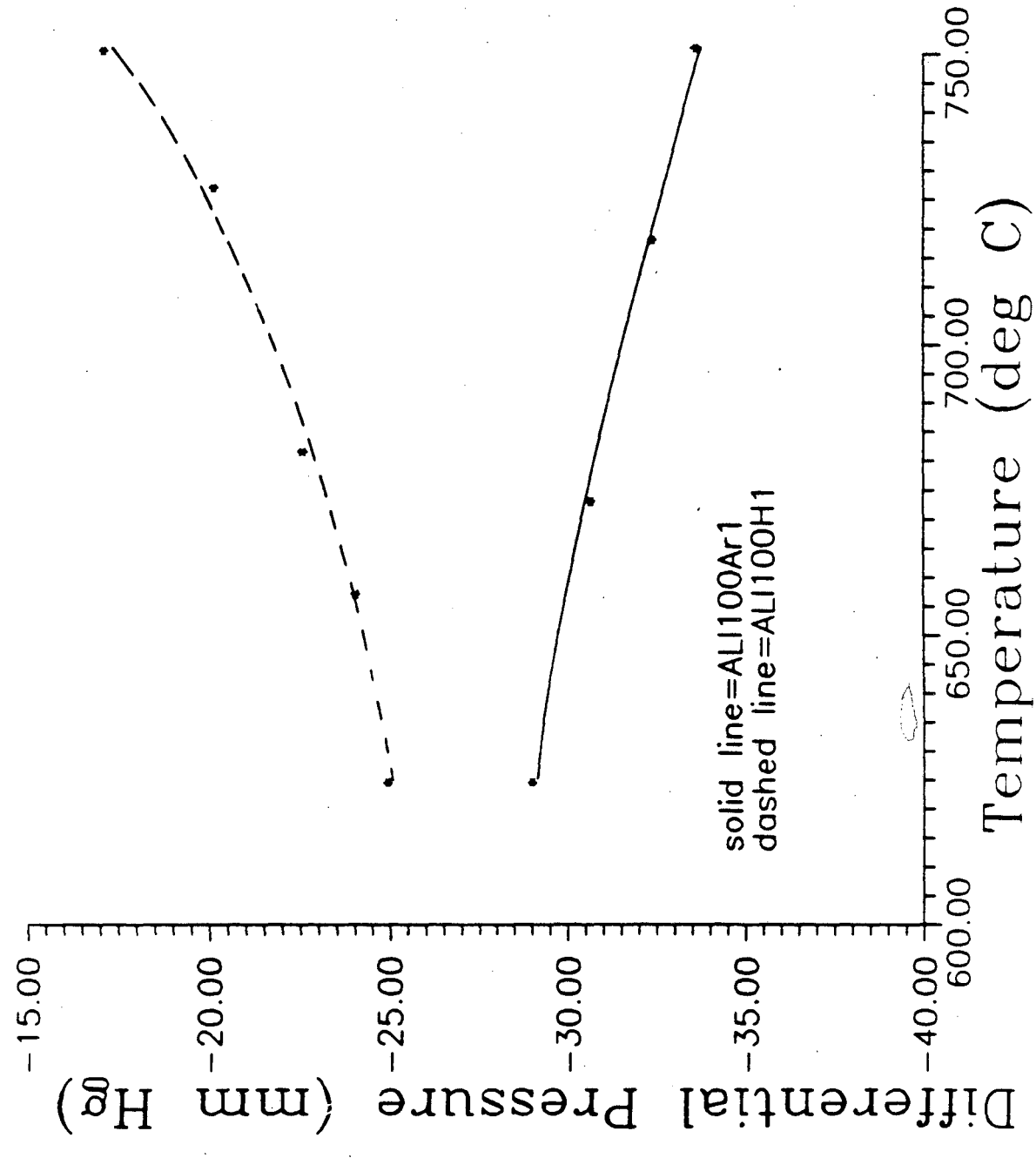

Fig. 4.7c Differential pressure for ampoules containing Al-Li alloy at P_{init} = 100 mm Hg

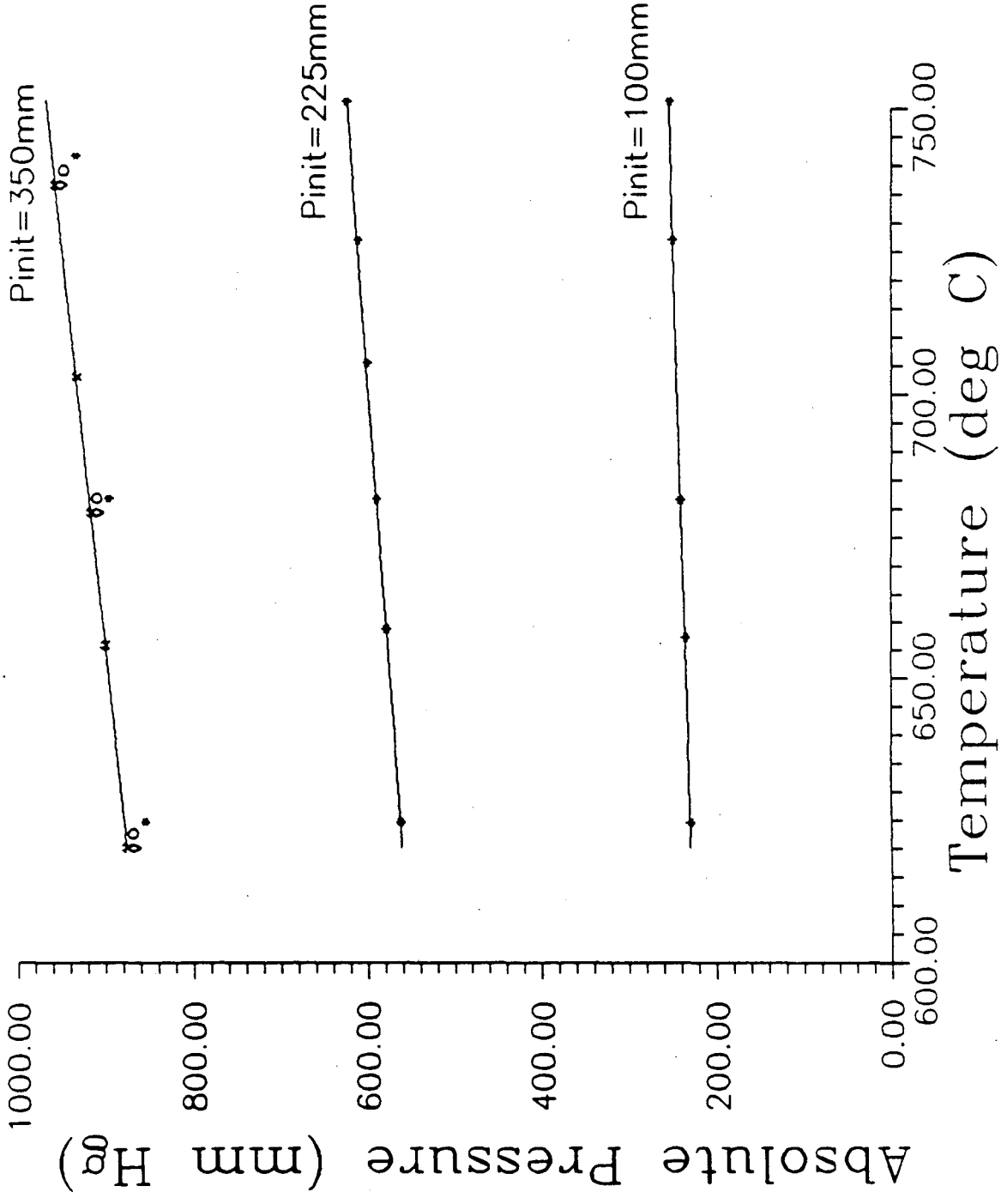

Fig. 4.8 Absolute pressure for experiments with Al-Li alloys for P_{init} of 100, 225 and 350 mm Hg

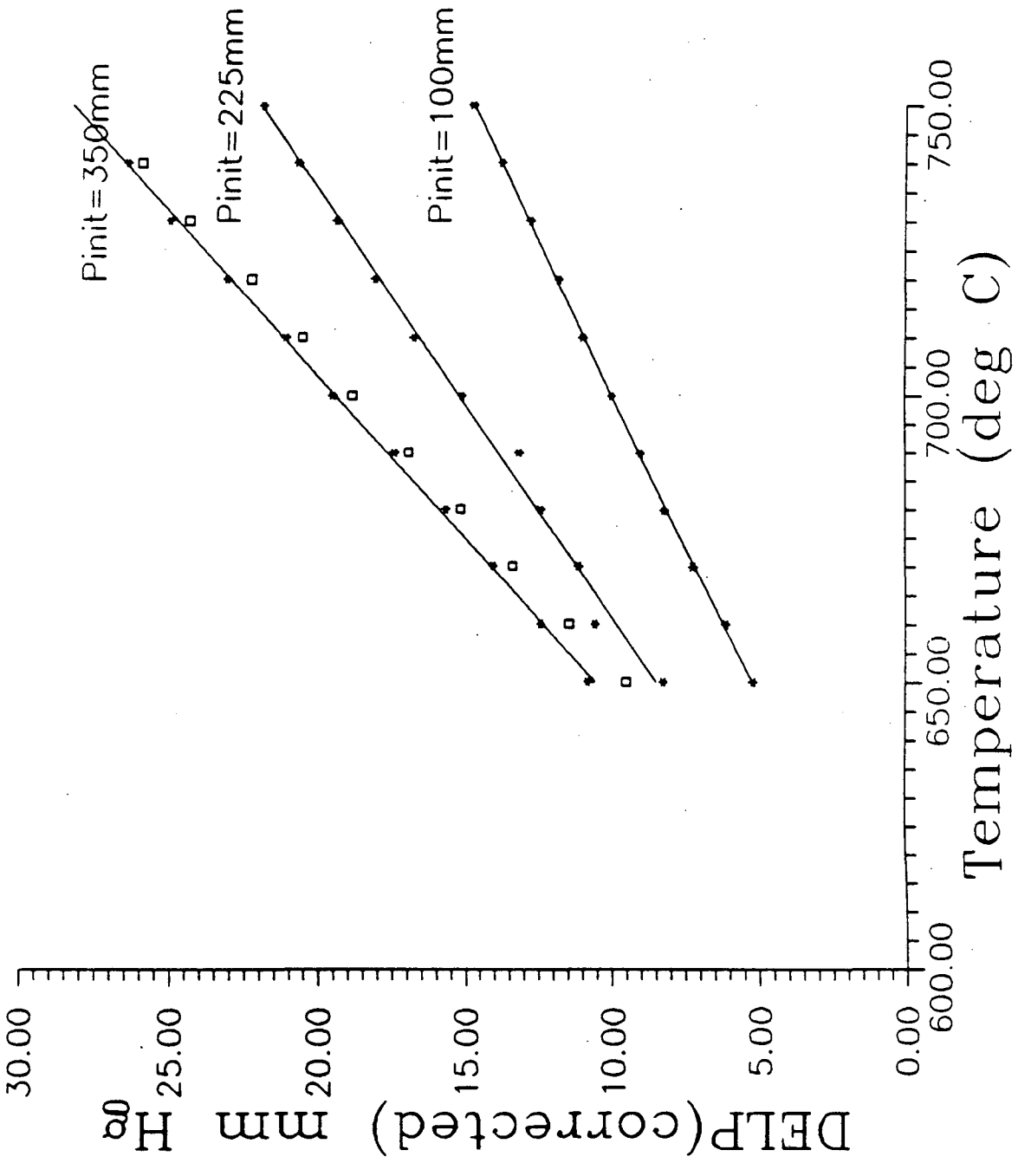

Fig. 4.9. ΔP (corrected) for experiments with Al-Li alloys for P_{init} of 100, 225 and 350 mm Hg

750°C are used and calculations are done for temperatures between 650°C – 750°C by fitting a curve through the observed data points and Figs. 4.9 – 4.11 are obtained from these). These ΔP values were used to calculate solubilities of hydrogen as shown in Appendix III.

For a diatomic gas such as H_2, the solubility is related to temperature by the expression:

$$S = S_o \exp (- \Delta H_s/2RT)$$

where S is the solubility of the gas, ΔH_s is the heat of solution of one mole of the gas, S_o is the pre-exponential constant and T is the absolute temperature. Therefore a plot of the log of solubility against reciprocal temperature should yield a straight line with slope of $- \Delta H_s/4.6R$.

Such plots have been made for the three runs and are shown in Fig. 4.10. All three runs yield straight lines of nearly equal slope. Values of ΔH_s have been calculated and are shown in Table 4.3, and are in reasonable agreement with each other.

TABLE 4.3

ΔH_s obtained from Fig. 4.11

P_{init}	ΔH^o (kJ mol^{-1})
100	145.33
225	133.86
350	137.68

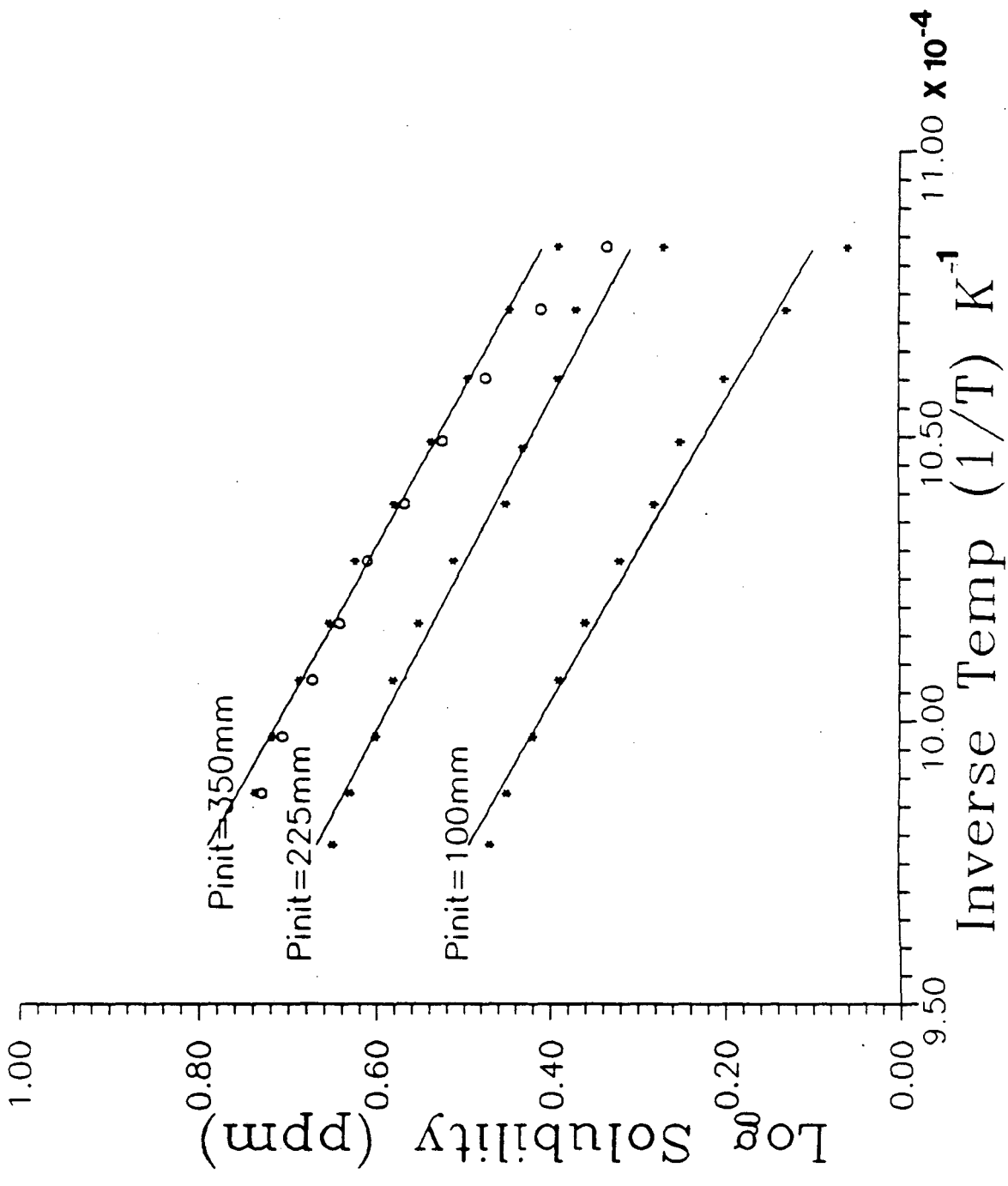

Fig. 4.10 **Arrhenius plot for solubility of hydrogen in liquid Al-Li alloys**

Reasonable agreement is seen between the various experimental runs.

Hydrogen dissolution in these alloys exhibited Sievert's law behavior, as shown in Fig. 4.11 in which a plot of the solubility of H_2 against the square root of the partial pressure of H_2 above the melt yields a straight line at a given temperature. This implies that molecular hydrogen dissociates to form atoms in solution.

A comparison of the hydrogen solubilties determined for the 2090 aluminum–lithium alloys with those for pure aluminum show that the solubility of hydrogen is about 4-6 times higher for the former. Two possible explanations can be offered – a very large increase in the solid solubility of hydrogen in the alloyed aluminum matrix by lithium addition or, and more likely, the formation of a hydrogen–rich phase in aluminum–lithium alloys during solidification. An example of a hydrogen–rich phase would be the hydride of lithium or lithium and aluminum, such as LiH or Li_3AlH_6. Considering the formation of LiH (1),

$$Li(1) + 1/2\ H_2(g) \longrightarrow LiH(1)$$

The heat of formation, ΔG° for this reaction is

$$\Delta G^\circ = -71\ 430 + 60.3T\ J\ mol^{-1} \quad [980 - 1100\ K]$$

Calculations show that for this reaction to occur, the equilibrium pressure of H_2 required is about 50 mm Hg at 1000 K(assuming $a_{LiH} = a_{Li} = 1$).

Since the experiment is carried out at pressures substantially

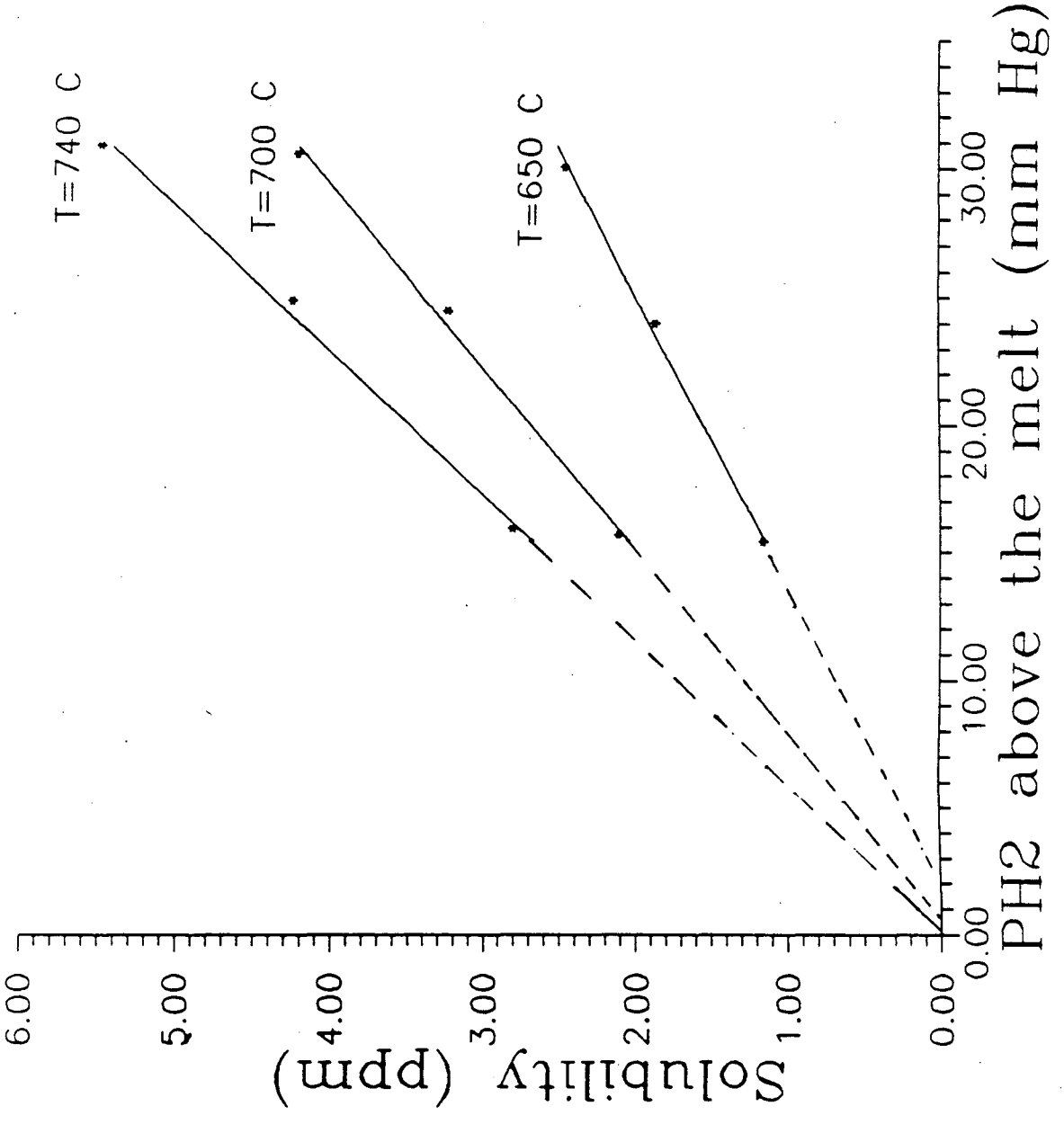

Fig. 4.11 Relationship between solubility of hydrogen in liquid Al-Li alloys and the square root of the hydrogen pressure above the melt

higher than this, the formation of lithium hydride is favored. This could be a possible explanation for our observations of the higher solubility of hydrogen in aluminum-lithium alloys. However, to detect the presence of the hydride phase, special techniques would have to be used as the crystal structures, lattice parameters and diffraction patterns of αAl and LiH are quite similar and would not be detected using standard microscopy techniques.(27)

Figs. 4.12 and 4.13 show the variations in absolute and differential pressure as a function of time at a given temperature. It is seen that equilibrium is asymptotically approached after 1-2 hours. This may be due to the formation of surface reaction products that inhibit the dissolution of hydrogen. This experiment used a static melt and resistance heating. It is thought that the use of an induction furnace would reduce equilibrium time by the stirring effect of induced fields.(3).

4.5 Error Estimates

The accuracy of the measurements involved is limited by
(i) the accuracy of the differential pressure transducer - the DPT is accurate upto 0.4mm Hg which translates into a variance of 0.10 - 0.12 ppm for temperatures in between 650 and 750°C.
(ii) the limitations of the process controller - the temperature can be measured with an accuracy of ± 2°C . This translates into a variance of 0.06 - 0.1 ppm when converted to solubility.

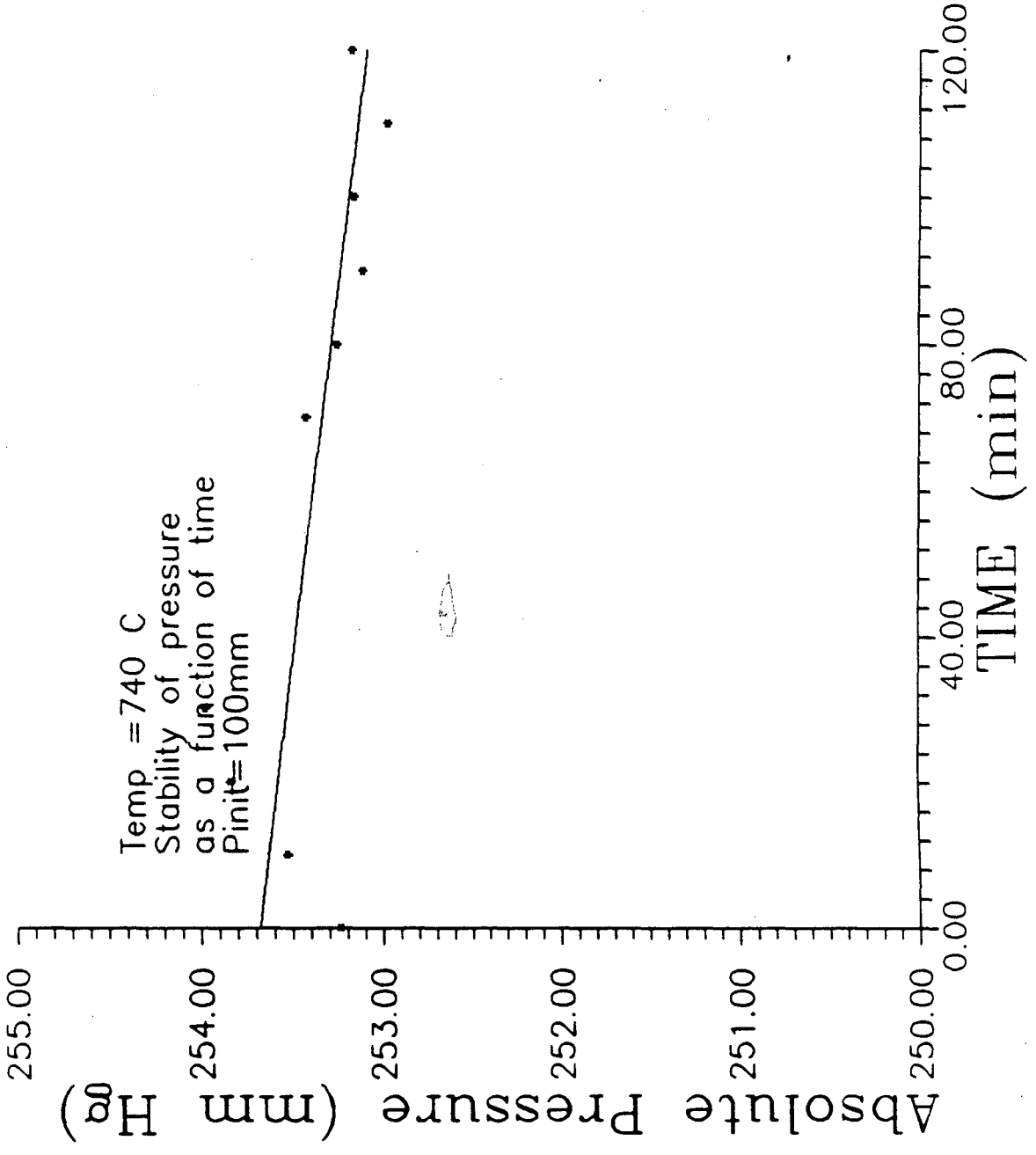

Fig. 4.12 Variation of absolute pressure with time for P_{init} = 100 mm Hg and T = 750°C

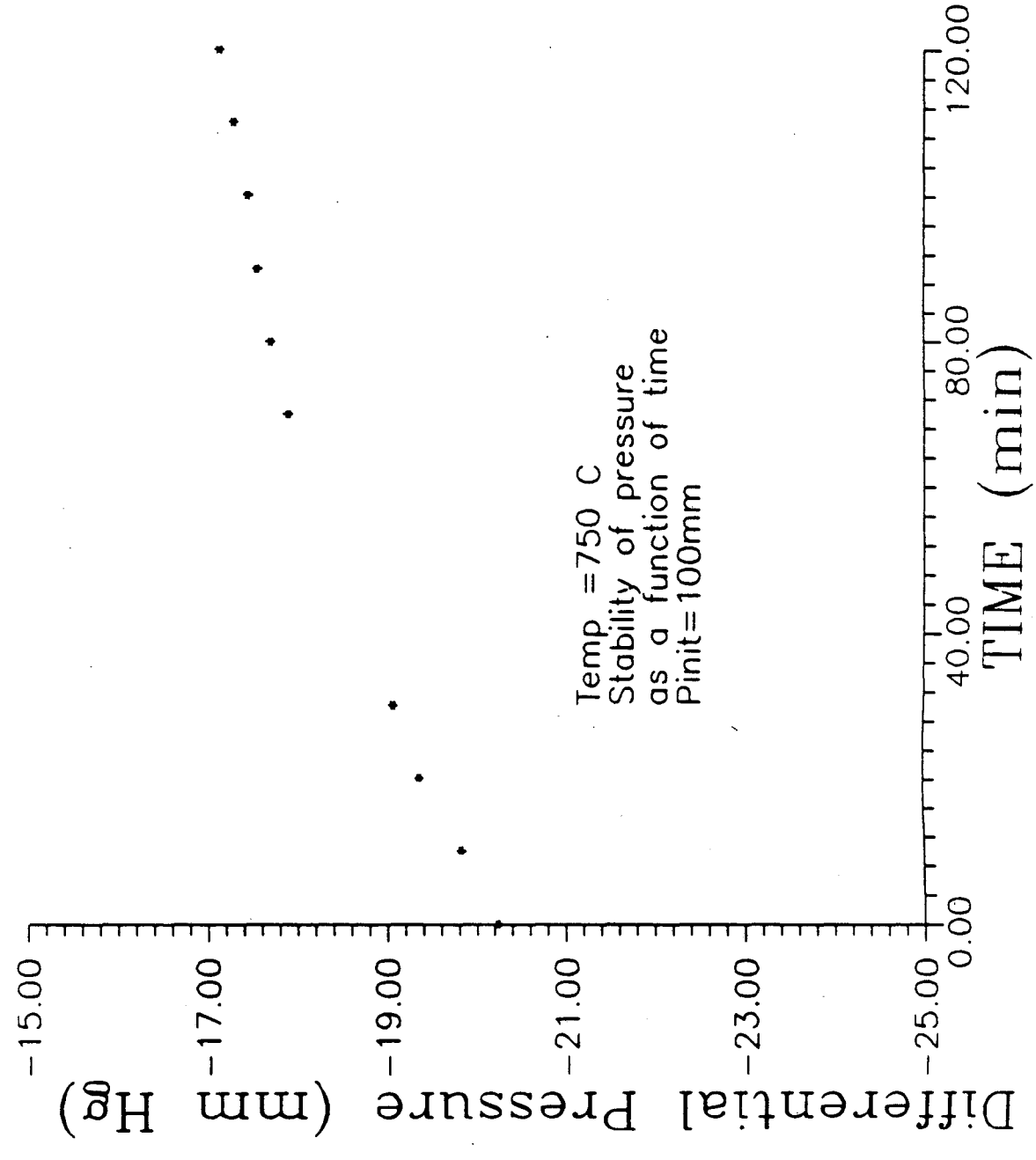

Fig. 4.13 Variation of differential pressure with time for P_{init} = 100 mm Hg and T = 750°C

(iii) the attainment of equilibrium – as discussed earlier, equilibrium is assumed when there is less than 0.4 mm Hg variation in the differential pressure which is the limit of the DPT.

With all these factors in mind, the accuracy of our experimental results is about $\pm$ 0.12 - 0.15 ppm which is less than 2% for the 350 mm run and about 4-5% for the 225 and 100 mm run.

5. CONCLUSIONS

(i) The constant volume technique can be used to determine solubility of gases in molten alloys. Certain improvements that can be incorporated in the experimental setup are

(a) use of induction heating to aid degassing and lower equilibration times

(b) investigation of the possibility of using metal/ceramic ampoules which will eliminate the glassblowing step and associated problems

(ii) Hydrogen solubility in 2090 aluminum lithium alloys (2.2 mass% Cu, 2.1 mass% Li) follows Sievert's law and dissolution takes place in atomic form.

(iii) The solubility of hydrogen in 2090 aluminum lithium alloys varies from 1-6 ppm for pressures of 250-950 mm Hg in the temperature range 650-750^{o}C.

(iv) The heat of dissolution of 2090 aluminum lithium alloys is around 135 kJ mol^{-1}.

(v) The solubility of hydrogen in 2090 aluminum lithium alloys is 4–6 times higher than the solubility of hydrogen in pure aluminum.

APPENDIX I

Design calculations for determining experimental volume

Factors considered as the basis of calculation were:

(i) Temperature Range: 650-750°C as discussed in section 3.2.

(ii) Weight of sample: assumed to be 5 grams

(iii) Estimated solubility of the alloys: assumed to be 0.5-5 ppm

Assuming 0.5 ppm hydrogen solubility, the amount of hydrogen dissolved is $0.5 \times 10^{-6} \times 5 = 2.5 \times 10^{-6}$ grams or 1.24×10^{-6} moles.

Similarly, for 5 ppm hydrogen solubility, the amount of hydrogen dissolved is 1.24×10^{-5} moles.

Using the ideal gas law,

$$\Delta P = \Delta nRT/V$$

where Δn = number of moles of hydrogen dissolved

R = gas constant = 62400 mm cm^3 mol^{-1} K^{-1}

T = absolute temperature in K

ΔP = pressure difference generated due to H_2 solubility in mm Hg

Using T = 1000 K, Table 3.1 is generated.

The effective volume of 50 cm^3 is a tradeoff between requirements of lower volume for accuracy and higher volume for ease of fabrication.

APPENDIX II

Derivation of the expression to account for pressure drop due to dead volume

The dead volume leads to a lower observed pressure than that predicted by ideal gas laws. The dead volume is defined here as that part of the experimental setup which lies in a non-isothermal zone. In this case, it has the following components:

- stainless steel tubing from the Swagelok fitting at the ampoule connection to the shutoff valve for both argon and hydrogen limbs
- stainless steel tubing from the DPT to both argon and hydrogen limbs (including the pressure port cavity volume of the DPT)
- stainless steel tubing from the APT to the argon limb (including the pressure port cavity of the APT)

Total dead volume for the argon limb is 6.143 cm^3 and for the hydrogen limb is 5.287 cm^3.

To derive an expression for the effect due to the dead volume the following assumptions were made:

(1) The dead volume, V_d, is at constant temperature and at ambient temperature throughout. This is not true in reality, but it is quite difficult to measure the temperature gradient in the dead volume. As seen in section 4, pressures predicted with this assumption corresponded satisfactorily to observed pressures.

(2) Gas does not dissolve in the ampoule or crucible.

For the sketch shown below, the number of moles of gas in the setup at $P_{initial}$, $T_{ambient}$ are

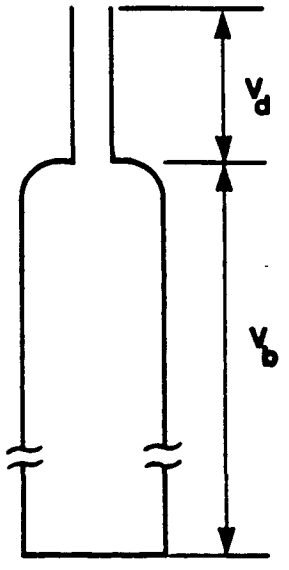

$$n_{initial} = \frac{P_{init}\ (V_d + V_b)}{RT_{amb}}$$

where V_b is the volume of the bulk and V_d is the dead volume.

At temperature T, the gas redistributes itself and the number of moles of gas in V_d is

$$n_d = \frac{PV_d}{RT_{amb}}$$

(since V_d is at T_{amb} throughout the experiment); and the number of moles of gas in V_b is

$$n_b = \frac{PV_b}{RT}$$

Since the system is closed, the number of moles of gas is constant. Therefore,

$$\frac{P_{init}\ (V_b + V_d)}{RT_{amb}} = \frac{P}{R}\left[\frac{V_d}{T_{amb}} + \frac{V_b}{T}\right]$$

which can be simplified to

$$\frac{P}{P_{init}} = \frac{V_d + V_b}{V_d + V_b\left[\frac{T_{amb}}{T}\right]}$$

When $V_d = 0$, this reduces to

$$\frac{P'}{P_{init}} = \frac{T}{T_{amb}}$$

where P' is the ideal gas pressure at constant volume.

We now define $\delta P = P - P'$

where P = observed pressure

P' = pressure predicted by ideal gas laws, with no dead volume

On making this substitution, we get

$$\frac{\delta P}{P_{init}} = T \left[\frac{V_d + V_b}{TV_d + V_b T_{amb}} - \frac{1}{T_{amb}} \right] \qquad \text{(A3)}$$

Expression A3 accounts for the deviation of the observed pressure from that predicted by ideal gas laws owing to the dead volume. This expression can be further manipulated to predict the dead volume and the pressure drop.

APPENDIX III

Typical Solubility Calculations

A typical calculation for the determination of solubility is shown below. Fig. A3.1 is a plot of differential pressures generated in experiments ali350ar2 and ali350h4 (refer Table 4.2). From Figs. A3.1 and 4.7 (pressure correction), we can generate values of differences in differential pressure (ΔP), as shown in the following table.

Table A3.1

ali350 calculations

T^oC	T^oK	$1/T\ K^{-1} \times 10^4$	ΔP_{obs} (mm)	ΔP_{corr} (mm)	ΔP_1(net) (mm)	S_1 (ppm)	$\log S_1$
650	923	10.83	17.70	6.90	10.81	2.46	0.39
660	933	10.72	19.67	7.26	12.41	2.79	0.46
670	943	10.60	21.64	7.63	14.01	3.12	0.49
680	953	10.49	23.61	8.00	15.61	3.44	0.54
690	963	10.38	25.74	8.36	17.37	3.79	0.58
700	973	10.28	28.20	8.73	19.47	4.20	0.62
710	983	10.17	30.16	9.10	21.07	4.50	0.65
720	999	10.07	32.46	9.46	23.03	4.87	0.69
730	1003	9.97	34.75	9.83	24.93	5.22	0.72
740	1013	9.87	36.56	10.20	26.36	5.46	0.74

Other information used in the generation of Table A3.1 are

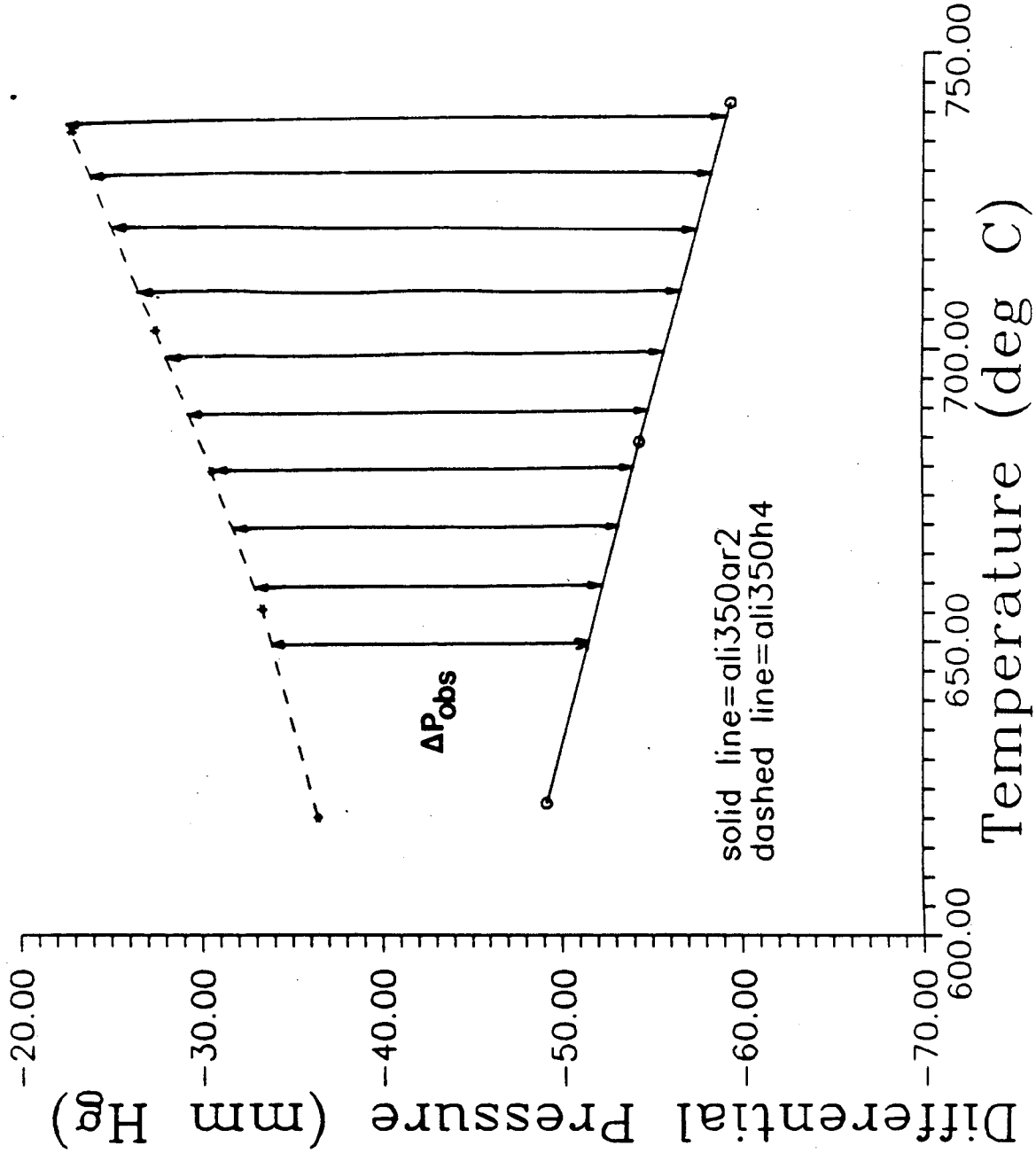

Fig. A3.1 Differential pressure for Al-Li alloy with P_{init} = 350 mm Hg

Vol of ampoule = 57.55 cm^3 (calculated)

= 57.25 cm^3 (measured)

dead volume = 5.49 cm^3 Vol of crucible = 6.62 cm^3

Total dead volume = 12.11 cm^3

Effective volume of ampoule = 45.44 cm^3

weight of alloy = 6.9954 gms

The solubility of hydrogen in the alloy, in parts per million, may be calculated from the following expression:

$$\text{Solubility} = \frac{\text{moles } H_2 \text{ dissolved x molecular weight of } H_2}{\text{mass of alloy}}$$

$$= \frac{\left[\frac{\Delta P_{l,net} \times V_{amp,eff}}{RT}\right] \times MW_{H_2}}{\text{mass of alloy}}$$

From Table A3.1, $\Delta P_{l,net}$ = 19.74 mm at 700°C

Substitution of appropriate values yields a solubility of 4.2 ppm.

REFERENCES

1. Gases in Carbons & Metals, Physics Data, 5-1 to 5-23, 1976.

2. L. I. Sokolskaya, Gases in Light Metals, Pergamon Press, 1961.

3. W. R. Opie and N. J. Grant, J. Metals, Vol. 188, 1950, p. 1237.

4. C. E. Ransley and H. Neufeld, J. Inst. Metals, August 1948, vol. 74, p. 599.

5. C. E. Ransley and D. E. J. Talbot, J. Inst. Metals, vol. 84, 1956, p. 445.

6. H. Aschehoug et al., Z. Metallkunde, Bd. 60, 1969, H. 11, p. 864.

7. J. L. Brandt and C. N. Cochran, J. Metals, December 1956, p. 1672.

8. C. E. Ransley, D. E. J. Talbot and H. C. Barlow, J. Inst. Metals, vol. 86, 1957, p. 212.

9. A. A. Grigoreva and V. A. Danelkin, Tsvetnye Met., 1974, pp.96-103.

10. F. Degreve et al., Met. Trans. 6B, Dec. 1975, p. 539.

11. F. Degreve et al., Met. Trans. 6B, Dec. 1975, p. 545.

12. F. Degreve et al., Met. Trans. 6B, Dec. 1975, p. 551.

13. R. Gee and D. J. Fray, Met. Trans. 9B, Sept. 1978, p. 427.

14. H.F. de Jong, Aluminium English, Vol 60 (1984), No 9 , pp. E587-E593

15. K. Welpmann, M. Peters and T.H. Sanders Jr., Aluminium English, Vol 60 (1984), No 10, pp E641–E646

16. Bulletin of Alloy Phase Diagrams, Vol 3, 1982 (2)

17. T. H. Sanders Jr. and E. A. Starke Jr., in Aluminum-Lithium I, Proc. 1st Intl. Aluminum-Lithium Conf., Stone Mountain, GA, May 1980, TMS-AIME, Warrendale, PA (1981), pp 1-15

18. W. J. Tomlinson, S. J. Kenney and N. Richards, Materials Chemistry and Physics, Vol 14, 1986, pp 393–396

19. T. H. Sanders Jr. and E. A. Starke Jr., (editors), ibid.

20. T. H. Sanders Jr. and E. A. Starke Jr. (editors), Aluminum–Lithium II, Proc. 2nd Intl. Aluminum–Lithium Conf., Monterey, CA, April 1983, TMS–AIME, Warrendale, PA (1984).

21. C. Baker, P. J. Gregson, S. J. Harris and C. J. Peel, Aluminium-Lithium Alloys III, Proc. 3rd Intl. Aluminium–Lithium Conf., Oxford, England 1985, The Institute of Metals (1986).

22. A. P. Divecha and S. D. Karmakar, ref. 17, pp 49–62.

23. W. A. Averill, D. L. Olson, D. E. Matlock and C. R. Edwards, ref. 17, pp.–28.

24. D. J. Field, E. P. Butler and G. M. Scamans, ref. 17, pp. 325-346.

25. D. J. Fields, G. M. Scamans and E. P. Butler, ref. 20, pp. 657-666.

26. D. J. Fields and E. P. Butler, ref. 20, pp. 667-673.

27. D. P. Hill, D. N. Williams and C. E. Mobley, ref. 17, pp. 201–218.

LAWRENCE BERKELEY LABORATORY
TECHNICAL INFORMATION DEPARTMENT
UNIVERSITY OF CALIFORNIA
BERKELEY, CALIFORNIA 94720